A genetically encoded fluorescent sensor for rapid and specific *in vivo* detection of norepinephrine

Jiesi Feng[1,2,3], Changmei Zhang[4,8], Julieta Lischinsky[5,9,10], Miao Jing[1,2,3], Jingheng Zhou[6], Huan Wang[1,2], Yajun Zhang[1,3,7], Ao Dong[1,2,3], Zhaofa Wu[1,2], Hao Wu[1,2,12], Weiyu Chen[4,8], Peng Zhang[7], Jing Zou[11], S. Andrew Hires[11], J. Julius Zhu[7,13,14,15], Guohong Cui[6], Dayu Lin[5,9,10], Jiulin Du[4,8], Yulong Li[1,2,3,16,*]

[1]State Key Laboratory of Membrane Biology, Peking University School of Life Sciences, Beijing 100871, China

[2]PKU-IDG/McGovern Institute for Brain Research, Beijing 100871, China

[3]Peking-Tsinghua Center for Life Sciences, Academy for Advanced Interdisciplinary Studies, Peking University, Beijing 100871, China

[4]Institute of Neuroscience, State Key Laboratory of Neuroscience, CAS Center for Excellence in Brain Science and Intelligence Technology, Chinese Academy of Sciences, Shanghai 200031, China

[5]Neuroscience Institute, New York University School of Medicine, New York, NY 10016, USA

[6]Neurobiology Laboratory, National Institute of Environmental Health Sciences, National Institutes of Health, Research Triangle Park, NC 27709, USA

[7]Department of Pharmacology, University of Virginia School of Medicine, Charlottesville, VA 22908, USA

[8]University of Chinese Academy of Sciences, Beijing 100049, China

[9]Department of Psychiatry, New York University School of Medicine, New York, NY 10016, USA

[10]Center for Neural Science, New York University, New York, NY 10016, USA

[11]Department of Biological Sciences, Neurobiology Section, University of Southern California, Los Angeles, CA 90089, USA

[12]School of Life Sciences, Tsinghua University, Beijing 100084, China

[13]School of Medicine, Ningbo University, Ningbo, 315010, China

[14]Donders Institute for Brain, Cognition and Behavior, Radboud University Nijmegen, 6525

32   EN, Nijmegen, Netherlands

33   [15]Department of Physiology, School of Basic Medicine, Tongji Medical College, Huazhong

34   University of Science and Technology, Wuhan 430030, China

35   [16]Lead contact

36

37   *Manuscript correspondence:

38   Yulong Li (yulongli@pku.edu.cn)

39

Acknowledgements

Author Contributions

Y. L conceived and supervised the project. J.F., M.J., H.Wang, A.D., and Z.W. performed experiments related to sensor development, optimization, and characterization in culture HEK cells, culture neurons and brain slices. Y.Z., P.Z. and J.J.Z designed and performed experiments using Sindbis virus in slices. C.Z., W.C., and J.D. designed and performed experiments on transgenic fish. J.L., J.Zhou, H.Wu, J.,Zou, S.A.H., G.C., and D.L. designed and performed experiments in behaving mice. All authors contributed to data interpretation and data analysis. Y. L and J.F. wrote the manuscript with input from M.J.,

67   J.L., and D.L. and help from other authors.

68

69   **Declaration of Interests**

70   The authors declare competing financial interests. J.F., M.J., H.Wang, and Y. L have filed

71   patent applications whose value might be affected by this publication.

72

Abstract

Norepinephrine (NE) and epinephrine (Epi), two key biogenic monoamine neurotransmitters, are involved in a wide range of physiological processes. However, their precise dynamics and regulation remain poorly characterized, in part due to limitations of available techniques for measuring these molecules *in vivo*. Here, we developed a family of GPCR Activation-Based NE/Epi (GRAB$_{NE}$) sensors with a 230% peak $\Delta F/F_0$ response to NE, good photostability, nanomolar-to-micromolar sensitivities, sub-second rapid kinetics, high specificity to NE vs. dopamine. Viral- or transgenic- mediated expression of GRAB$_{NE}$ sensors were able to detect electrical-stimulation evoked NE release in the locus coeruleus (LC) of mouse brain slices, looming-evoked NE release in the midbrain of live zebrafish, as well as optogenetically and behaviorally triggered NE release in the LC and hypothalamus of freely moving mice. Thus, GRAB$_{NE}$ sensors are a robust tool for rapid and specific monitoring of *in vivo* NE/Epi transmission in both physiological and pathological processes.

Introduction

Both norepinephrine (NE) and epinephrine (Epi) are key monoamine neurotransmitters in the central nervous systems and peripheral organs of vertebrate organisms. These transmitters play an important role in a plethora of physiological processes, allowing the organism to cope with its ever-changing internal and external environment. In the brain, NE is synthesized primarily in the locus coeruleus (LC), a small yet powerful nucleus located in the pons. Noradrenergic LC neurons project throughout the brain and exert a wide range of effects, including processing sensory information (Berridge and Waterhouse, 2003), regulating the sleep-wake/arousal state (Berridge et al., 2012), and mediating attentional function (Bast et al., 2018). Blocking noradrenergic transmission causes impaired cognition and arousal and is closely correlated with a variety of psychiatric conditions and neurodegenerative diseases, including stress (Chrousos, 2009), anxiety (Goddard et al., 2010), depression (Moret and Briley, 2011), attention-deficit hyperactivity disorder (ADHD) (Berridge and Spencer, 2016), and Parkinson's disease (PD) (Espay et al., 2014). In the sympathetic nervous system, both NE and Epi play a role in regulating heart function (Brodde et al., 2001) and blood pressure (Zimmerman, 1981).

Despite their clear importance in a wide range of physiological processes, the spatial and temporal dynamics of NE and Epi in complex organs (*e.g.* the vertebrate brain) are poorly understood at the *in vivo* level due to limitations associated with current detection methods. Classic detection methods such as microdialysis-coupled biochemical analysis (Bito et al., 1966; Justice, 1993; Watson et al., 2006) have low temporal resolution, requiring a relatively long time (typically 5 min/collection) and complex sampling procedures, thereby limiting the ability to accurately measure the dynamics of noradrenergic activity in the physiological state (Chefer et al., 2009). Recent improvements in microdialysis—in particular, the introduction of the nano-LC-microdialysis method (Lee et al., 2008; Olive et al., 2000)—have significantly increased detection sensitivity; however, this approach is still limited by a relatively slow sampling rate (on the order of several minutes). On the other hand, electrochemical detection techniques based on measuring currents generated by the oxidation of NE/Epi (Bruns, 2004; Park et al., 2009; Robinson et al., 2008; Zhou and Misler, 1995) provide nanomolar sensitivity and millisecond temporal resolution; however, their inability to distinguish NE and Epi from other monoamine neurotransmitters— particularly dopamine (Robinson et al., 2003)—presents a significant physiological limitation with respect to measuring noradrenergic/adrenergic transmission both in *ex vivo* tissue preparations and *in vivo*. In addition, both microdialysis-based and electrochemical techniques are designed to detect volume-averaged NE/Epi levels in the extracellular fluid and therefore cannot provide cell type–specific or subcellular information.

Real-time imaging of NE dynamics would provide an ideal means to non-invasively track NE with high spatiotemporal resolution. A recent innovation in real-time imaging, the cell-based reporters known as CNiFERs (Muller et al., 2014), converts an extracellular NE signal into an intracellular calcium signal that can be measured using highly sensitive

128 fluorescence imaging. However, CNiFERs require implantation of exogenous cells and can
129 report only volume transmission of NE/Epi. By contrast, genetically encoded sensors, in
130 theory, circumvent the above-mentioned limitations to provide fast, clear, non-invasive, cell
131 type–specific reporting of NE/Epi dynamics. In practice, all genetically encoded NE sensors
132 developed to date have poor signal-to-noise ratio and narrow dynamic range (*e.g.*, a <10%
133 change in FRET ratio under optimal conditions) (Nakanishi et al., 2006; Vilardaga et al.,
134 2003; Wang et al., 2018b), thus limiting their applicability, particularly in *in vivo* applications.

135 To overcome these limitations, we developed a series of genetically encoded single-
136 wavelength fluorescent GRAB$_{NE}$ sensors with rapid kinetics, a $\Delta F/F_0$ dynamic range of
137 ~200%, and EGFP-comparable spectra, brightness, and photostability. Here, we
138 showcase the wide applicability of our GRAB$_{NE}$ sensors using a number of *in vitro* and *in*
139 *vivo* preparations. In every application tested, the GRAB$_{NE}$ sensors readily reported robust,
140 chemical-specific NE signals. Thus, our GRAB$_{NE}$ sensors provide a powerful imaging-
141 based probe for measuring the cell-specific regulation of adrenergic/noradrenergic
142 transmission under a wide range of physiological and pathological conditions.

143

Results

Development and characterization of GRAB$_{NE}$ sensors

Inspired by the structure (Rasmussen et al., 2011a; Rasmussen et al., 2011b) and working mechanism (Chung et al., 2011; Manglik et al., 2015; Nygaard et al., 2013) of the β2 adrenergic G protein–coupled receptor (GPCR), we exploited the conformational change between the fifth and sixth transmembrane domains (TM5 and TM6, respectively) upon ligand binding to modulate the brightness of an attached fluorescent protein. Building upon the successful strategy of generating GPCR activation-based sensors for acetylcholine (GACh) (Jing et al., 2018) and dopamine (GRAB$_{DA}$) (Sun et al., 2018), we first systematically screened human adrenergic receptors as a possible scaffold. We inserted circular permutated EGFP (cpEGFP) into the third intracellular loop domain (ICL3) of three α-adrenergic receptors (α1DR, α2AR, and α2BR) and two β-adrenergic receptors (β2R and β3R) (Fig. 1A). Among these five constructs, we found that α2AR-cpEGFP had the best membrane trafficking, indicated by its high colocalization with membrane-targeted RFP (Fig. S1); we therefore selected this construct as the scaffold for further screening.

The length of the linker surrounding the cpEGFP moiety inserted in G-GECO (Zhao et al., 2011), GCaMP (Akerboom et al., 2012), GACh (Jing et al., 2018), and GRAB$_{DA}$ (Sun et al., 2018) can affect the fluorescence response of cpEGFP-based indicators. Thus, as the next step, we systematically truncated the linker which starts with the entire flexible ICL3 of α2AR surrounding cpEGFP (Fig. 1B). We initially screened 275 linker-length variant proteins and identified a sensor (GRAB$_{NE0.5m}$) with a modest response to NE (Fig. 1B, right). From this scaffold, we performed a random mutation screening of seven amino acids (AAs) in close proximity to the cpEGFP moiety; two of these AAs are on the N-terminal side of cpEGFP, and the remaining five are on the C-terminal side of cpEGFP (Fig. 1C). From approximately 200 mutant versions of GRAB$_{NE0.5m}$, we found that GRAB$_{NE1m}$—which contains a glycine-to-threonine mutation at position C1—provided the best performance with respect to ΔF/F$_0$ and brightness (Fig. 1C, middle and right).

Next, we expressed GRAB$_{NE1m}$ in HEK293T cells and applied NE in a range of concentrations. NE induced a fluorescence change in GRAB$_{NE1m}$-expressing cells in a dose-dependent manner, with an EC$_{50}$ of 0.93 μM and a maximum ΔF/F$_0$ of approximately 230% in response to a saturating concentration of NE (100 μM) (Fig. 1D, middle and right). We also introduced mutations in α2AR in order to increase its sensitivity at detecting NE. We found that a single T6.34K point mutation (Ren et al., 1993)—which is close to the highly conserved E6.30 site—resulted in a 10-fold increase in sensitivity (EC$_{50}$ ~83 nM) to NE compared with GRAB$_{NE1m}$; this sensor, which we call GRAB$_{NE1h}$, has a maximum ΔF/F$_0$ of ~130% in response to 100 μM NE. As a control, we also generated GRAB$_{NEmut}$, which has the mutation S5.46A at the putative ligand-binding pocket and therefore is unable to bind NE (Fig. 1D); this control sensor has similar brightness and membrane trafficking (Fig. S1 and S2A), but does not respond to NE even at 100 μM (Fig. 1D, middle and right).

To examine whether our GRAB$_{NE}$ sensors can capture the rapid dynamic properties of NE signaling, including its release, recycling, and degradation, we bathed GRAB$_{NE1h}$-expressing HEK293T cells in a solution containing NPEC-caged NE; a focused spot of 405-nm light was applied to locally uncage NE by photolysis (Fig. 2A). Transient photolysis induced a robust increase in fluorescence in GRAB$_{NE1h}$-expressing cells (mean on time constant 137ms, single exponential fit), which was blocked by application of the α2-adrenergic receptor antagonist yohimbine (Fig. 2B,C). To characterize both the on and off rates (τ_{on} and τ_{off}, respectively) of the GRAB$_{NE}$ sensors, we locally applied various compounds to GRAB$_{NE}$-expressing cells using rapid perfusion and measured the fluorescence response using high-speed line scanning (Fig. 2D,E). The average delay intrinsic to the perfusion system (measured by fitting the fluorescence increase in the co-applied red fluorescent dye Alexa 568) was 34 ms (Fig. 2F). Fitting the fluorescence change in each sensor with a single exponential function yielded an average τ_{on} of 72 and 36 ms for GRAB$_{NE1m}$ and GRAB$_{NE1h}$, respectively, and an average τ_{off} of 680 and 1890 ms for GRAB$_{NE1m}$ and GRAB$_{NE1h}$, respectively (Fig. 2E,F). The faster on-rate and slower off-rate of GRAB$_{NE1h}$ compared to GRAB$_{NE1m}$ is consistent with its relatively higher affinity for NE.

High ligand specificity is an essential requirement for tools designed to detect structurally similar monoamine-based molecules. Importantly, our GRAB$_{NE}$ sensors, which are based on α2AR, respond to both NE and Epi, but do not respond to other neurotransmitters (Fig. 2G). The sensors also respond to the α2AR agonist brimonidine but not the β2-adrenergic receptor agonist isoprenaline, which indicates receptor-subtype specificity. Moreover, the NE-induced fluorescence increase in GRAB$_{NE}$-expressing cells was blocked by the α-adrenergic receptor antagonist yohimbine, but not the β-adrenergic receptor antagonist ICI 118,551. Additionally, because NE and DA are structurally similar yet functionally distinct, we characterized how our GRAB$_{NE}$ sensors respond to various concentrations of DA and NE. Wild-type α2AR has an 85-fold higher affinity for NE versus DA (Fig. 2H, right); in contrast, GRAB$_{NE1m}$ has a 350-fold higher affinity for NE, whereas GRAB$_{NE1h}$ was similar to the wild-type receptor, with a 37-fold higher affinity for NE (Fig. 2H). In contrast, fast-scan cyclic voltammetry (FSCV) was unable to differentiate between NE and DA, producing a nearly identical response to similar concentrations of NE and DA (Fig. 2I) (Robinson et al., 2003). To test the photostability of our NE sensors, we continuously illuminated GRAB$_{NE}$-expressing HEK293T cells using either 1-photon (confocal) or 2-photon laser microscopy and found that the GRAB$_{NE}$ sensors are more photostable than EGFP under both conditions (Fig. S2C). Taken together, these data suggest that the GRAB$_{NE}$ sensors can be used to measure the dynamic properties of noradrenergic activity with high specificity for NE over other neurotransmitters.

Next, we examined whether our GRAB$_{NE}$ sensors can trigger GPCR-mediated downstream signaling pathways. First, we bathed GRAB$_{NE1m}$-expressing cells in a saturating concentration of NE for 2 h, but found no significant internalization of GRAB$_{NE1m}$ (Fig. 2J).

8

223   Similarly, we found that both GRAB$_{NE1m}$ and GRAB$_{NE1h}$ lack β-arrestin–mediated signaling,
224   even at the highest concentration of NE tested (Fig. 2K), suggesting that the GRAB$_{NE}$
225   sensors are not coupled to β-arrestin signaling. In addition, GRAB$_{NE1m}$ and GRAB$_{NE1h}$ had
226   drastically reduced downstream Gi coupling compared to wild-type α2AR, which was
227   measured using a Gi-coupling–dependent luciferase complementation assay (Fig. 2L)
228   (Wan et al., 2018). We also found that G protein activation by GRAB$_{NE1m}$ measured using
229   the highly sensitive TGFα shedding was reduced by about 100-fold compared to the wild-
230   type receptor (Fig. S2B) (Inoue et al., 2012). Finally, blocking G protein activation by
231   treating cells with pertussis toxin (Fig. 2M) had no effect on the fluorescence response of
232   either GRAB$_{NE1m}$ or GRAB$_{NE1h}$, indicating that the fluorescence response of GRAB$_{NE}$
233   sensors does not require G protein coupling (Rasmussen et al., 2011a). Taken together,
234   these data indicate that GRAB$_{NE}$ sensors can be used to report NE concentration without
235   inadvertently engaging GPCR downstream signaling.

236

237   **_Characterization of GRAB$_{NE}$ sensors in cultured neurons_**

238   The expression, trafficking, and response of proteins can differ considerably between
239   neurons and cell lines (Marvin et al., 2013; Zou et al., 2014). Therefore, to characterize the
240   performance of GRAB$_{NE}$ sensors in neurons, we co-expressed GRAB$_{NE}$ together with
241   several neuronal markers in cultured cortical neurons. Both GRAB$_{NE1m}$ and GRAB$_{NEmut}$
242   trafficked to the cell membrane and co-localized with the membrane-targeted marker RFP-
243   CAAX (Fig. 3A,B). Upon bath-application of a saturating concentration of NE, GRAB$_{NE1m}$
244   and GRAB$_{NE1h}$ had a peak $\Delta F/F_0$ of approximately 230% and 150%, respectively, whereas
245   GRAB$_{NEmut}$ had no response (Fig. 3D,E); these results are similar to our results obtained
246   with HEK293T cells. Moreover, the NE-induced response in GRAB$_{NE1m}$-expressing cells
247   was similar among various subcellular compartments identified by co-expressing
248   GRAB$_{NE1m}$ with either the axonal marker synaptophysin (SYP) or the dendritic marker
249   PSD95 suggesting that GRAB$_{NE}$ sensors enable the detection of NE throughout the
250   neurons (Fig. 3C). Both GRAB$_{NE1m}$- and GRAB$_{NE1h}$-expressing neurons had a dose-
251   dependent fluorescence increase in response to NE, with mean EC$_{50}$ values of 1.9 μM and
252   93 nM, respectively (Fig. 3F). Consistent with high selectivity for NE, GRAB$_{NE1m}$ and
253   GRAB$_{NE1h}$ have a 1000-fold and 7-fold higher affinity, respectively, for NE versus DA (Fig.
254   3F). Moreover, GRAB$_{NE1m}$ responded specifically to NE and Epi, but did not respond to
255   several other neurotransmitters and ligands, including the β2-adrenergic receptor agonist
256   isoprenaline, histamine, dopamine, and serotonin (Fig. 3G). Finally, culturing GRAB$_{NE1m}$-
257   expressing neurons in 100 μM NE for one hour did not cause internalization of the sensor,
258   and the fluorescence increase was both stable for the entire hour and blocked completely
259   by the α2-adrenergic receptor antagonist yohimbine (Fig. 3H,I). Thus, our GRAB$_{NE}$ sensors
260   have the necessary affinity and specificity to faithfully measure noradrenergic signaling in
261   neurons.

Characterization of GRAB$_{NE}$ sensors in both cultured and acute brain slices

To further test the GRAB$_{NE}$ sensors *in vitro*, we expressed GRAB$_{NE1m}$ and GRAB$_{NE1h}$ in cultured hippocampal slices using a Sindbis virus expression system (Fig. S3A). In both GRAB$_{NE1m}$-expressing CA1 neurons and GRAB$_{NE1h}$-expressing CA1 neurons, exogenous application of NE in ACSF—but not ACSF alone—evoked a robust increase in fluorescence (Fig. S3B-D). In contrast, NE had no detectable effect on GRAB$_{NEmut}$-expressing neurons (Fig. S3C,D). Application of several α-adrenergic receptor agonists, including epinephrine and brimonidine, also generated a fluorescence increase in GRAB$_{NE1m}$-expressing neurons (Fig. S3C,F), consistent with data obtained using cultured cells. The rise and decay kinetics of the change in fluorescence were second-order, which reflects the integration of the time required to puff the drugs onto the cells and the sensor's response kinetics (Fig. S3E,G). We also prepared acute hippocampal slices in which GRAB$_{NE1h}$ was expressed using an adeno-associated virus (AAV); in this acute slice preparation, the GRAB$_{NE1h}$-expressing hippocampal neurons are innervated by noradrenergic fibers, which was confirmed by post-hoc staining using an antibody against dopamine beta hydroxylase (Fig. S3H,I). Application of electrical stimuli at 20 Hz for 1 s elicited a robust increase in GRAB$_{NE1h}$ fluorescence, and this increase was blocked by the application of yohimbine (Fig. S3J). Consistent with our results obtained using cultured slices, exogenous application of various α-adrenergic receptor agonists, including NE, Epi, and brimonidine— but not the β-adrenergic receptor agonist isoprenaline—evoked a fluorescence increase in GRAB$_{NE1h}$-expressing neurons, and this response was blocked by yohimbine, but not by the β-adrenergic receptor antagonist ICI 118,551 (Fig. S3K).

Next, we examined whether our GRAB$_{NE}$ sensors can be used to monitor the dynamics of endogenous NE. We expressed GRAB$_{NE1m}$ in the locus coeruleus (LC), which contains the majority of adrenergic neurons within the brain (Fig. 4A). Two weeks after AAV injection, we prepared acute brain slices and observed GRAB$_{NE1m}$ expression in the membrane of LC neurons using two-photon microscopy (Fig. 4A). We then used electrical stimuli to evoke the release of endogenous NE in the LC in the acute slices. Applying one or two stimuli did not produce a detectable fluorescence increase in GRAB$_{NE1m}$-expressing neurons; in contrast, applying 10 or more stimuli at 20 Hz caused a progressively stronger response (Fig. 4B). Application of the voltage-activated potassium channel blocker 4-aminopyridine, which increases Ca^{2+} influx during the action potential, significantly increased the fluorescence response, whereas application of Cd^{2+} to block calcium channels abolished the stimulation-induced fluorescence increase (Fig. 4C), consistent with presynaptic NE release being mediated by Ca^{2+} influx. We also performed line-scanning experiments in order to track the kinetics of NE release (Fig. 4D, left). A brief electrical stimulation induced a rapid fluorescence response with a mean τ_{on} and τ_{off} of 37 ms and 600 ms, respectively (Fig. 4D, middle and right). Taken together, these data indicate that GRAB$_{NE1m}$ can be used to monitor the release of endogenous NE in real time.

10

302   NE released into the synapse is recycled back into the presynaptic terminal by the
303   norepinephrine transporter (NET). We therefore tested the sensitivity of GRAB$_{NE1m}$ to NET
304   blockade using desipramine. In the presence of desipramine, electrical stimuli caused a
305   larger fluorescence response in GRAB$_{NE1m}$-expressing neurons compared to ACSF alone
306   (Fig. 4E). Moreover, desipramine significantly slowed the τ_{off} of the fluorescence signal,
307   consistent with reduced reuptake of extracellular NE into the presynaptic terminal. To rule
308   out the possibility that the change in the fluorescence response was caused by a change
309   in synaptic modulation over time, we applied repetitive electrical stimuli at 5-min intervals
310   to GRAB$_{NE1m}$-expressing neurons and found that the stimulation-evoked response was
311   stable for up to 40 min (Fig. 4F). Finally, we examined the specificity of the stimulation-
312   induced response. Compared with a robust response in control conditions, the α-
313   adrenergic antagonist yohimbine blocked the response; moreover, no response was
314   elicited in LC neurons expressing GRAB$_{NEmut}$ or in LC neurons expressing a dopamine
315   version of the sensor (GRAB$_{DA1m}$) (Fig. 4G). In contrast, cells expressing GRAB$_{DA1m}$
316   responded robustly to the application of DA, and the GRAB$_{NE1m}$ and GRAB$_{DA1m}$ responses
317   were abolished by yohimbine and the dopamine receptor antagonist haloperidol,
318   respectively (Fig. 4H). Taken together, these data indicate that GRAB$_{NE1m}$ is both sensitive
319   and specific for detecting endogenous noradrenergic activity in LC neurons.

320

GRAB$_{NE1m}$ detects both exogenous NE application and endogenous NE release in awake zebrafish

323   Zebrafish is both a genetically accessible vertebrate species and an optically transparent
324   organism, thus serving as a suitable model for *in vivo* imaging. We generated the
325   transgenic zebrafish line Tg(HuC:NE1m), which pan-neuronally expresses the GRAB$_{NE1m}$
326   sensor. Pan-neuronal expression was confirmed by GRAB$_{NE1m}$ fluorescence on the cell
327   membrane of neurons throughout the brain (Fig. 5A). Bath application of 50 μM NE—but
328   not DA at the same concentration—elicited a robust increase in fluorescence intensity that
329   was blocked completely by the subsequent application of 50 μM yohimbine (Fig. 5B-D). In
330   addition, a separate zebrafish line expressing GRAB$_{NEmut}$ did not respond to NE (Fig. 5C,D).
331   Taken together, these data indicate that GRAB$_{NE1m}$ can be used to measure NE in an *in*
332   *vivo* model.

333   Next, we investigated whether GRAB$_{NE1m}$ can be used to measure the dynamics of
334   endogenous noradrenergic activity induced by a visual looming stimulus, which triggers a
335   robust escape response in zebrafish. We applied repetitive looming stimuli while using
336   confocal imaging to measure the fluorescence of GRAB$_{NE1m}$-expressing neurites in the
337   optic tectum (Fig. 5E). Each looming stimulus induced a time-locked increase in GRAB$_{NE1m}$
338   fluorescence, which was blocked by bath application of yohimbine but was unaffected by
339   the β-adrenergic receptor antagonist ICI 118,551 (Fig. 5F,G). In contrast, the same looming
340   stimuli had no effect in animals expressing GRAB$_{NEmut}$ (Fig. 5F,G). In addition, adding

11

341 desipramine to block NE reuptake slowed the decay of the fluorescence signal (Fig. 5H).

342 By sparse expression of GRAB$_{NE1m}$ in individual neurons in zebrafish larvae via transient

343 transfection, we were also able to record robust signals corresponding to NE release at

344 single-cell resolution in response to repetitive looming stimuli (Fig. 5I-K), confirming that

345 our GRAB$_{NE}$ sensors can be used to sense NE release at a single-cell level with high

346 spatiotemporal resolution.

347

348 **GRAB$_{NE1m}$ detects optogenetically evoked NE release in freely moving mice**

349 Having demonstrated the proof-of-concept in a relatively simple *in vivo* vertebrate system,

350 we next examined whether the GRAB$_{NE}$ sensors can be used to monitor the noradrenergic

351 activity in the mammalian brain by virally expressing GRAB$_{NE1m}$ (non-Cre dependent)

352 together with the optogenetic actuator C1V1 (Cre-dependent) in the LC of Th-Cre mice

353 (Fig. 6A). Optogenetic stimulation of LC NE neurons using 561 nm laser pulses reliably

354 evoked an increase in GRAB$_{NE1m}$ fluorescence in fiber photometry recording of freely

355 moving mice. Moreover, Intraperitoneal (i.p.) injection of desipramine produced a slow

356 progressive increase in basal GRAB$_{NE1m}$ fluorescence (consistent with an increase in

357 extracellular NE levels) and caused an increase in the magnitude and decay time of the

358 light-activated responses. I.p. injection of yohimbine abolished both the increase in basal

359 GRAB$_{NE1m}$ fluorescence and the light-evoked responses (Fig. 6B-D). In contrast, treating

360 mice with either GBR 12909 (a selective blocker of dopamine transporters) or eticlopiride

361 (a specific D2R antagonist) had no effect on the light-evoked responses in GRAB$_{NE1m}$

362 fluorescence (Fig. 6C-E). To further test the selectivity of GRAB$_{NE1m}$ between NE and

363 dopamine, we co-expressed GRAB$_{NE1m}$ and DIO-C1V1 both in the LC and in the substantia

364 nigra pars compacta (SNc) of Th-Cre mice (Fig. 6F). In these mice, optogenetic stimulation

365 of dopamine neurons in the SNc did not cause any changes in the GRAB$_{NE1m}$ fluorescence

366 in the SNc. In contrast, stimulating NE neurons in the LC produced a clear increase in

367 GRAB$_{NE1m}$ fluorescence (Fig. 6F, G). These results confirm that the increase of GRAB$_{NE1m}$

368 fluorescence reflects the release of endogenous NE from noradrenergic neurons in the LC.

369

370 **Using GRAB$_{NE1m}$ to track endogenous NE dynamics in the mouse hypothalamus**

371 **during freely moving behaviors**

372 In the brain, the hypothalamus mediates a variety of innate behaviors essential for survival,

373 including feeding, aggression, mating, parenting, and defense (Hashikawa et al., 2016;

374 Sokolowski and Corbin, 2012; Yang and Shah, 2016). The hypothalamus receives

375 extensive noradrenergic projections (Moore and Bloom, 1979; Schwarz and Luo, 2015;

376 Schwarz et al., 2015) and expresses an abundance of α2-adrenergic receptors (Leibowitz,

377 1970; Leibowitz et al., 1982). Microdialysis studies found that the hypothalamus is among

378 the brain regions that contains high level of NE during stress (McQuade and Stanford,

12

379   2000; Pacak et al., 1995; Shekhar et al., 2002; Tanaka, 1999). To better understand the
380   dynamics of NE signaling in the hypothalamus under stress, we virally expressed hSyn-
381   GRAB$_{NE1m}$ in the lateral hypothalamus of C57BL/6 mice. Three weeks after virus injection,
382   we performed fiber photometry recordings of GRAB$_{NE1m}$ fluorescence during a variety of
383   stressful and non-stressful behaviors in freely moving mice (Fig. 7).

384   During forced swim test and tail suspension test (both of which were stressful), we
385   observed a significant increase in GRAB$_{NE1m}$ fluorescence. During forced swim test, the
386   fluorescence signal increased continuously regardless of the animal's movements and
387   started to decrease only after the animal was removed from the water (Fig. 7C1-E1). During
388   the 60-s tail suspension test, the signal began to rise when the animal was first pursued
389   by the experimenter's hand, increased continuously while the animal was suspended by
390   the tail, and decreased rapidly back to baseline levels when the animal was returned to its
391   home cage (Fig. 7C2-E2). Additionally, when a human hand was placed in front of the
392   animal, we observed a small and transient increase in GRAB$_{NE1m}$ fluorescence (Fig. 7C3-
393   E3). In contrast, the presence of a non-aggressive mouse of either the same or the
394   opposite sex or close social interaction with the conspecific (7C4-E4, C5-E5) caused no
395   significant change in GRAB$_{NE1m}$ fluorescence. Lastly, neither sniffing nor eating a food
396   attractant—in this case, peanut butter—had an effect on GRAB$_{NE1m}$ fluorescence (Fig.
397   7C6-E6). These data provide evidence that noradrenergic activity in the lateral
398   hypothalamus occurs primarily under stressful conditions.

399   Finally, to confirm that the GRAB$_{NE1m}$ sensor indeed detects changes in NE concentration
400   instead of other monoamine neurotransmitters, such as dopamine, we injected mice with
401   a specific NET inhibitor atomoxetine (3 mg/kg i.p.) to inhibit the reuptake of NE. Although
402   atomoxetine had no effect on the peak change in GRAB$_{NE1m}$ fluorescence during the tail
403   suspension test, it significantly slowed the return to baseline levels after each tail
404   suspension (Fig. 7F1-I1); in contrast, treating mice with the α-adrenergic receptor
405   antagonist yohimbine (2 mg/kg) both decreased the peak change in GRAB$_{NE1m}$
406   fluorescence and significantly accelerated the return to baseline (Fig. 7F1-I1). Treating
407   mice with either the selective DAT inhibitor GBR 12909 (10 mg/kg, i.p.) or the D2 receptor
408   antagonist sulpiride (50 mg/kg, i.p.) had no effect on the peak change in GRAB$_{NE1m}$
409   fluorescence or the time to return to baseline (Fig. 7F2-I2). In summary, these data
410   demonstrate that our GRAB$_{NE}$ sensors are suitable for monitoring endogenous
411   noradrenergic activity in real time, with high spatiotemporal precision, during freely
412   moving behavior in mammals.

Discussion

Here, we report the development and validation of $GRAB_{NE1m}$ and $GRAB_{NE1h}$, two genetically encoded norepinephrine/epinephrine sensors that can be used both *in vitro* and *in vivo* to monitor noradrenergic activity with high temporal and spatial resolution, high ligand specificity, and cell type specificity. In mouse acute brain slices, our $GRAB_{NE}$ sensors detected NE release from the LC in response to electrical stimulation. In zebrafish, the $GRAB_{NE}$ sensors reported looming-induced NE release with single-cell resolution. In mice, the $GRAB_{NE}$ sensors reported the time-locked release of NE in the LC triggered by optogenetic stimulation, as well as changes in hypothalamic NE levels during a variety of stress-related behaviors.

Compared to existing methods for detecting NE, our $GRAB_{NE}$ sensors have several distinct advantages. First, NE has been difficult to distinguish from DA *in vivo* (*e.g.* by fast-scan cyclic voltammetry) (Park et al., 2009; Robinson et al., 2003), largely because of their structural similarities with only one hydroxyl group difference. Our $GRAB_{NE}$ sensors have extremely high *specificity* for NE over other neurotransmitters and chemical modulators, including DA (Figs. 2H, 3F). $GRAB_{NE1m}$ has a roughly 1000-fold higher affinity for NE over DA when expressed in neurons, even better than the 85-fold difference of the wild-type α2-adrenergic receptor. Thus, our $GRAB_{NE}$ sensors provide new opportunities to probe the dynamics of noradrenergic activity with high specificity, which is particularly valuable when studying the many brain regions that receive overlapping dopaminergic and noradrenergic inputs. One thing to note is that $GRAB_{NE}$ sensors are engineered from the α2a receptor, which may not be suitable for pharmacological investigation of α2a receptor related regulations.

Second, our $GRAB_{NE}$ sensors have extremely high *sensitivity* for NE. Specifically, the EC_{50} for NE approaches sub-micromolar levels, with a 200%—or higher—increase in fluorescence intensity upon binding NE. By comparison, recently published FRET-based NE indicators produce a signal change of ≤10% under optimal conditions (Wang et al., 2018a; Wang et al., 2018b). Thus, $GRAB_{NE}$ sensors have much improved characteristics to monitor endogenous *in vivo* NE dynamics. Third, $GRAB_{NE}$ sensors have brightness and photostability properties that rival EGFP, which permits stable recordings across extended experimental sessions. Fourth, because they provide sub-second response kinetics and are genetically encoded, our $GRAB_{NE}$ sensors can non-invasively report noradrenergic activity *in vivo* with single-cell resolution and a high recording rate (~30 Hz). Finally, because the $GRAB_{NE}$ sensors can traffic to various surface membranes, including the cell body, dendrites, and axons, and because they perform equally well in these membrane compartments, they can provide subcellular spatial resolution, which is essential for understanding compartmental NE signaling *in vivo*.

Ligand binding to endogenous GPCRs drives G-protein activation and receptor internalization. If present in $GRAB_{NE}$ sensors, these responses could interfere with

14

452 endogenous signaling fidelity and disrupt normal neuronal activity. To assess this risk, we
453 characterized the downstream coupling of our GRAB$_{NE}$ sensors with both G protein–
454 independent and G protein–dependent pathways. Importantly, the introduction of the
455 cpEGFP moiety in the GRAB$_{NE}$ sensors resulted in non-detectable engagement of
456 arrestin-mediated desensitization/internalization, which ensures more consistent surface
457 expression of the sensor and that the GRAB$_{NE}$ sensors do not inadvertently activate
458 arrestin-dependent signaling. With respect to G protein–dependent signaling, we found
459 that although physiological levels of NE robustly induce a change in GRAB$_{NE1m}$
460 fluorescence, they do not engage downstream G protein signaling (Fig. 2J-M).

461 Noradrenergic projections throughout the brain originate almost exclusively from the LC,
462 and NE release plays a role in a wide range of behaviors, including cognition and the
463 regulation of arousal, attention, and alertness (Berridge and Waterhouse, 2003; Li et al.,
464 2018; Schwarz et al., 2015). In this respect, it is interesting to note that our *in vivo*
465 experiments revealed that GRAB$_{NE}$ sensors can reliably report looming-evoked NE release
466 in the optic tectum of live zebrafish. Moreover, our fiber photometry recordings of GRAB$_{NE}$
467 sensors in the hypothalamus of freely behaving mice revealed specific changes in
468 noradrenergic activity under stressful conditions (e.g., a tail lift or forced swimming),
469 whereas non-stressful conditions such as feeding and social interaction did not appear to
470 alter noradrenergic activity. These data are generally consistent with previous data
471 obtained using microdialysis to measure NE (McQuade and Stanford, 2000; Pacak et al.,
472 1995; Shekhar et al., 2002; Tanaka, 1999). Importantly, however, our approach yielded a
473 more temporally precise measurement of noradrenergic activity with the promise of higher
474 spatial and cell-type specificity.

475 NE circuits of the LC receive heterogeneous inputs from a broad range of brain regions
476 and send heterogeneous outputs to many brain regions (Schwarz et al., 2015).
477 Congruously, altered noradrenergic activity has been associated with a broad range of
478 brain disorders and conditions, including ADHD, PD, depression, and anxiety (Marien et
479 al., 2004). The complexity of these disorders may, in part, reflect the complexities of
480 noradrenergic circuits and signals, which previous tools have been unable to fully dissect.
481 Thus, understanding the regulation and impact of noradrenergic activity during complex
482 behavior demands technological advances, such as the GRAB$_{NE}$ sensors we present here.
483 Deploying these in concert with other cell-specific tools for reporting (Jing et al., 2018;
484 Patriarchi et al., 2018; Sun et al., 2018) and manipulating neurotransmitter levels (Fenno
485 et al., 2011; Urban and Roth, 2015) should increase our understanding of the circuits and
486 mechanisms that underlie brain functions in both health and diseases.

15

Experimental model and subject details

Primary cultures

Rat cortical neurons were prepared from postnatal day 0 (P0) Sprague-Dawley rat pups (both male and female, randomly selected; Beijing Vital River). In brief, cortical neurons were dissociated from dissected P0 rat brains in 0.25% Trypsin-EDTA (Gibco), plated on 12-mm glass coverslips coated with poly-D-lysine (Sigma-Aldrich), and cultured at 37°C in 5% CO_2 in neurobasal medium (Gibco) containing 2% B-27 supplement, 1% GlutaMax, and 1% penicillin-streptomycin (Gibco).

Cell lines

HEK293T cells were obtained from ATCC (CRL-3216) and verified based on their morphology under the microscope and by their growth curve. Stable cell lines expressing the wild-type α2-adrenergic receptor or various $GRAB_{NE}$ sensors were constructed by co-transfecting cells with the pPiggyBac plasmid carrying target genes with Tn5 transposase into a stable HEK293T-based cell line expressing chimeric Gαq/i and AP-TGFα (Inoue et al., 2012). Cells that stably expressed the target genes were selected by treating with 2 mg/ml Puromycin (Sigma) after reaching 100% confluence. The HTLA cells used for the TANGO Assay stably express a tTA-dependent luciferase reporter and a β-arrestin2-TEV fusion gene and were a gift from Bryan L. Roth (Kroeze et al., 2015). All cell lines were cultured at 37°C in 5% CO_2 in DMEM (Gibco) supplemented with 10% (v/v) fetal bovine serum (Gibco) and 1% penicillin-streptomycin (Gibco).

Mice

All procedures regarding animals were approved by the respective Animal Care and Use Committees at Peking University, New York University, University of Southern California and the US National Institutes of Health, and were performed in compliance with the US National Institutes of Health guidelines for the care and use of laboratory animals. Wild-type Sprague-Dawley rat pups (P0) were used to prepare cultured cortical neurons. Wild-type C57BL/6 and Th-Cre mice (MMRRC_031029-UCD, obtained from MMRRC) were used to prepare the acute brain slices and for the *in vivo* mouse experiments. Experimental Th-Cre mice were produced by breeding Th-Cre hemizygous BAC transgenic mice with C57BL/6J mice. All animals were housed in the animal facility and were family-housed or pair-housed in a temperature-controlled room with a 12hr-12h light-dark cycle (10 pm to 10 am light) with food and water provided *ad libidum*. All *in vivo* mouse experiments were performed using 2-12-month-old mice of both sexes.

Zebrafish

The background strain for these experiments is the albino strain slc45a2b4. To generate transgenic zebrafish, Both the pTol2-HuC:$GRAB_{NE1m}$ plasmid and Tol2 mRNA were co-injected into single-cell stage zebrafish eggs, and the founders of HuC:NE1m were

524 screened. HuC:NEmut transgenic fish were generated as described above using the
525 pTol2-HuC:GRAB$_{NEmut}$ plasmid. Adult fish and larvae were maintained on a 14h-10h
526 light-dark cycle at 28°C. All experimental larvae were raised to 6-8 days post-fertilization
527 (dpf) in 10% Hank's solution, which consisted of (in mM): 140 NaCl, 5.4 KCl, 0.25
528 Na$_2$HPO$_4$, 0.44 KH$_2$PO$_4$, 1.3 CaCl$_2$, 1.0 MgSO$_4$, and 4.2 NaHCO$_3$ (pH 7.2). Larval
529 zebrafish do not undergo sex differentiation prior to 1 month post-fertilization (Singleman
530 and Holtzman, 2014).

531

Method details

Molecular cloning

534 The molecular clones used in this study were generated by Gibson Assembly using DNA
535 fragments amplified using primers (Thermo Fisher Scientific) with 25-bp overlap. The
536 Gibson Assembly cloning enzymes consisted of T5-exonuclease (New England Biolabs),
537 Phusion DNA polymerase (Thermo Fisher Scientific), and Taq ligase (iCloning). Sanger
538 sequencing was performed using the sequencing platform at the School of Life Sciences
539 of Peking University in order to verify the sequence of all clones. All cDNAs encoding the
540 candidate GRAB$_{NE}$ sensors were cloned into the pDisplay vector (Invitrogen) with an
541 upstream IgK leader sequence and a downstream IRES-mCherry-CAAX cassette to label
542 the cell membrane. The cDNAs of select adrenergic receptor candidates were amplified
543 from the human GPCR cDNA library (hORFeome database 8.1), and cpEGFP from
544 GCaMP6s was inserted into the third intracellular loop (ICL3). The insertion sites for the
545 GRAB$_{NE}$ sensors were screened by truncating the ICL3 of the α2-adrenergic receptor at
546 the 10-amino acid (AA) level, followed by fine-tuning at the 1-AA level. Coupling linkers
547 were randomized by PCR amplification using randomized NNB codons in target sites.
548 Other cDNAs used to express the GRAB$_{NE}$ sensors in neurons were cloned into the pAAV
549 vector using the human synapsin promoter (hSyn) or TRE promoter. pAAV-CAG-tTA was
550 used to drive expression of the TRE promoter. The plasmids carrying compartmental
551 markers were cloned by fusing EGFP-CAAX, RFP-CAAX (mScarlet), KDELR-EGFP,
552 PSD95-RFP, and synaptophysin-RFP into the pDest vector. To characterize signaling
553 downstream of the GRAB$_{NE}$ sensors, we cloned the sensors and the wild-type α2-
554 adrenergic receptor into the pTango and pPiggyBac vector, respectively. GRAB$_{NE1m}$-SmBit
555 and α2AR-SmBit constructs were derived from β2AR-SmBit (Wan et al., 2018) using a
556 BamHI site incorporated upstream of the GGSG linker. LgBit-mGsi was a gift from Nevin
557 A. Lambert.

Expression of GRAB$_{NE}$ sensors in cultured cells and in vivo

559 The GRAB$_{NE}$ sensors were characterized in HEK293T cells and cultured rat cortical
560 neurons, with the exception of the TANGO assay and TGFα shedding assay. HEK293T
561 cells were passaged with Trypsin-EDTA (0.25%, phenol red; Gibco) and plated on 12-mm

17

562   size 0 glass coverslips in 24-well plates and grown to ~70% confluence for transfection.

563   HEK293T cells were transfected by incubating cells with a mixture containing 1 µg of DNA

564   and 3 µg of PEI for 6 h. Imaging was performed 24-48 h after transfection. Cells expressing

565   GRAB$_{NE}$ sensors for screening were plated on 96-well plates (PerkinElmer).

566   Cultured neurons were transfected using the calcium phosphate method at 7-9 DIV. In brief,

567   the neurons were incubated for 2 h in a mixture containing 125 mM $CaCl_2$, HBS (pH 7.04),

568   and 1.5 µg DNAh. The DNA-$Ca_3(PO4)_2$ precipitate was then removed from the cells by

569   washing twice with warm HBS (pH 6.80). Cells were imaged 48 h after transfection.

570   For *in vivo* expression, the mice were anesthetized by an i.p. injection of 2,2,2-

571   tribromoethanol (Avetin, 500 mg/kg body weight, Sigma-Aldrich), and then placed in a

572   stereotaxic frame for injection of AAVs using a Nanoliter 2000 Injector (WPI) or Nanoject II

573   (Drummond Scientific) microsyringe pump. For the experiments shown in Figures 4 and 6,

574   the AAVs containing hSyn-GRAB$_{NE1m/NE1mut/DA1m}$ and Ef1a-DIO-C1V1-YFP were injected

575   into the LC (AP: -5.45 mm relative to Bregma; ML: ±1.25 mm relative to Bregma; and DV:

576   -2.25 mm from the brain surface) or SNc (AP: -3.1 mm relative to Bregma; ML: ±1.5 mm

577   relative to Bregma; and DV: -3.8 mm from the brain surface) of wild-type or Th-Cre mice.

578   For the experiments shown in Figure 7, 100 nl of AAV9-hSyn-GRAB$_{NE1m}$ (Vigene, 1×10^{13}

579   titer genomic copies per ml) were unilaterally into the hypothalamus (AP: -1.7 mm relative

580   to Bregma; ML: 0.90 mm relative to Bregma; and DV: -6.05 mm from the brain surface) of

581   wild-type (C57BL/6) mice at a rate of 10 nl/min.

582   ***Fluorescence imaging of HEK293T cells and cultured neurons***

583   HEK293T cells and cultured neurons expressing GRAB$_{NE}$ sensors were screened using

584   an Opera Phenix high-content imaging system (PerkinElmer) and imaged using an inverted

585   Ti-E A1 confocal microscope (Nikon). A 60x/1.15 NA water-immersion objective was

586   mounted on the Opera Phenix and used to screen GRAB$_{NE}$ sensors with a 488-nm laser

587   and a 561-nm laser. A 525/50 nm and a 600/30 nm emission filter were used to collect the

588   GFP and RFP signals, respectively. HEK293T cells expressing GRAB$_{NE}$ sensors were first

589   bathed in Tyrode's solution and imaged before and after addition of the indicated drugs at

590   the indicated concentrations. The change in fluorescence intensity of the GRAB$_{NE}$ sensors

591   was calculated using the change in the GFP/RFP ratio. For confocal microscopy, the

592   microscope was equipped with a 40x/1.35 NA oil-immersion objective, a 488-nm laser, and

593   a 561-nm laser. A 525/50 nm and a 595/50 nm emission filter were used to collect the GFP

594   and RFP signals, respectively. GRAB$_{NE}$-expressing HEK293T cells and neurons were

595   perfused with Tyrode's solutions containing the drug of interest in the imaging chamber.

596   The photostability of GRAB$_{NE}$ sensors and EGFP was measured using a confocal

597   microscope (for 1-photon illumination) equipped with a 488-nm laser at a power setting of

598   ~350 µW, and using a FV1000MPE 2-photon microscope (Olympus, 2-photon illumination)

599   equipped with a 920-nm laser at a power setting of ~27.5 mW. The illuminated region was

600   the entire HEK293T cell expressing the target protein, with an area of ~200 µm^2. Photolysis

601 of NPEC-caged-NE (Tocris) was performed by combining fast scanning with a 76-ms pulse
602 of 405-nm laser illumination by a confocal microscope.

TANGO assay

604 NE at various concentrations (ranging from 0.1 nM to 100 μM) was applied to α2AR-
605 expressing or NE1m-/NE1h-expressing HTLA cells (Kroeze et al., 2015). The cells were
606 then cultured for 12 hours to allow expression of the luciferase gene. Furimazine (NanoLuc
607 Luciferase Assay, Promega) was then applied to a final concentration of 5 μM, and
608 luminescence was measured using a VICTOR X5 multilabel plate reader (PerkinElmer).

TGFα shedding assay

610 Stable cell lines expressing Gαi-AP-TGFα together with the wild-type α2AR or GRAB$_{NE}$
611 sensors were plated in a 96-well plate and treated by the addition of 10 μl of a 10x solution
612 of NE in each well, yielding a final NE concentration ranging from 0.1 nM to 100 μM.
613 Absorbance at 405 nm was read using a VICTOR X5 multilabel plate reader (PerkinElmer).
614 TGFα release was calculated as described previously (Inoue et al., 2012). Relative levels
615 of G protein activation were calculated as the TGFα release of GRAB$_{NE}$ sensors normalized
616 to the release mediated by wild-type α2AR.

FSCV

618 Fast-scan cyclic voltammetry was performed using 7-μm carbon fiber microelectrodes.
619 Voltammograms were measured with a triangular potential waveform from −0.4 V to +1.1
620 V at a scan rate of 400 V/s and a 100-ms interval. The carbon fiber microelectrode was
621 held at −0.4 V between scans. Voltammograms measured in the presence of various
622 different drugs in Tyrode's solution were generated using the average of 200 scans
623 followed by the subtraction of the average of 200 background scans. Currents were
624 recorded using the Pinnacle tethered FSCV system (Pinnacle Technology). Pseudocolor
625 plots were generated using Pinnacle FSCV software. The data were processed using Excel
626 (Microsoft) and plotted using Origin Pro (OriginLab).

Luciferase complementation assay

628 The luciferase complementation assay was performed as previously described (Wan et al.,
629 2018). In brief, ~48h after transfection the cells were washed with PBS, harvested by
630 trituration, and transferred to opaque 96-well plates containing diluted NE solutions.
631 Furimazine (Nano-Glo; 1:1000; Promega) was added to each well immediately prior to
632 performing the measurements with Nluc.

Fluorescence imaging of GRAB$_{NE}$ in brain slices

634 Fluorescence imaging of acute brain slices was performed as previously described (Sun
635 et al., 2018). In brief, the animals were anesthetized with Avertin, and acute brain slices
636 containing the LC region or the hippocampus region were prepared in cold slicing buffer

637 containing (in mM): 110 choline-Cl, 2.5 KCl, 1.25 NaH_2PO_4, 25 $NaHCO_3$, 7 $MgCl_2$, 25
638 glucose, and 2 $CaCl_2$. Slices were allowed to recover at 35°C in oxygenated Ringers
639 solution containing (in mM): 125 NaCl, 2.5 KCl, 1.25 NaH_2PO_4, 25 $NaHCO_3$, 1.3 $MgCl_2$,
640 25 glucose, and 2 $CaCl_2$ for at least 40 minutes before experiments. An Olympus
641 FV1000MPE two-photon microscope equipped with a 40x/0.80 NA water-immersion
642 objective and a mode-locked Mai Tai Ti:Sapphire laser (Spectra-Physics) tuned to 920
643 nm were used for imaging the slices. For electrical stimulation, a concentric electrode
644 (model #CBAEC75, FHC) was positioned near the LC region, and the imaging and
645 stimuli were synchronized using an Arduino board controlled using a custom-written
646 program. The imaging speed was set at 0.148 s/frame with 128 x 96 pixels in each frame.
647 The stimulation voltage was set at ~6 V, and the duration of each stimulation was
648 typically 1 ms. Drugs were either delivered via the perfusion system or directly bath-
649 applied in the imaging chamber.

650 For immunostaining of brain sections, $GRAB_{NE}$-expressing mice were anesthetized with
651 Avetin, and the heart was perfused with 0.9% NaCl followed by 4% paraformaldehyde
652 (PFA). The brain was then removed, placed in 4% PFA for 4 h, and then cryoprotected
653 in 30% (w/v) sucrose for 24 h. The brain was embedded in tissue-freezing medium, and
654 50-μm thick coronal sections were cut using a Leica CM1900 cryostat (Leica, Germany).
655 A chicken anti-GFP antibody (1:500, Abcam, #ab13970) was used to label $GRAB_{NE}$, and
656 a rabbit anti-DBH antibody (1:50, Abcam, #ab209487) was used to label adrenergic
657 terminals in the hippocampus. Alexa-488-conjugated goat-anti-chicken and Alexa-555-
658 conjugated goat-anti-rabbit secondary antibodies were used as the secondary antibody,
659 and the nuclei were counterstained with DAPI. The sections were imaged using a
660 confocal microscope (Nikon).

661 ***Fluorescence imaging of zebrafish***

662 Tg(HuC:GRAB-NE$_{1m}$) zebrafish larvae were imaged by using an upright confocal
663 microscope (Olympus FV1000, Japan) equipped with a 20x water-dipping objective
664 (0.95 NA). The larvae were first paralyzed with α-bungarotoxin (100 μg/ml, Sigma),
665 mounted dorsal side up in 1.5% low melting-point agarose (Sigma), and then perfused
666 with an extracellular solution consisting of (in mM) 134 NaCl, 2.9 KCl, 4 $CaCl_2$, 10
667 HEPES, and 10 glucose (290 mOsmol/L, pH 7.8). Images were acquired at 1-2 Hz with
668 a view field of 800 × 800 pixels and a voxel size was 0.62 × 0.62 × 2.0 μm^3 (x × y × z).
669 To detect the sensor's response to exogenous NE, 50 μM L-(-)-norepinephrine (+)-
670 bitartrate salt monohydrate (Sigma) in 5 μM L-ascorbic acid and 50 μM yohimbine
671 hydrochloride (TOCRIS) were sequentially applied to the bath. To detect endogenous NE
672 release, visual looming stimuli, which mimic approaching objects or predators (Yao et al.,
673 2016) were projected to the larvae under a red background. Each trial lasted 5 s, and 5
674 trials were performed in a block, with a 90-s interval between trials. To examine the
675 specificity of responses, ICI 118,551 hydrochloride (50 μM, Sigma) and desipramine
676 hydrochloride (50 μM, Sigma) were applied. Looming stimuli in transiently transfected

20

677   HuC:GRAB$_{NE1m}$ zebrafish were measured at single-cell resolution by using the same

678   conditions described above.

Fiber photometry recording in freely moving mice during optical stimulation

680   In the all-optic experiments shown in Figure 6, multimode optical fiber probes (105/125 μm

681   core/cladding) were implanted into the LC (AP: -5.45 mm relative to Bregma; ML: ±0.85

682   mm relative to Bregma; and DV: -3.5 mm from the brain surface) and the SNc (AP: -3.1

683   mm relative to Bregma; ML: ±1.5 mm relative to Bregma; and DV: -3.85 mm from the brain

684   surface) in mice four weeks after viral injection. Fiber photometry recording in the LC and/or

685   SNc was performed using a 473-nm laser with an output power of 25 μW measured at the

686   end of the fiber. The measured emission spectra were fitted using a linear unmixing

687   algorithm   (https://www.niehs.nih.gov/research/atniehs/labs/ln/pi/iv/tools/index.cfm).   The

688   coefficients generated by the unmixing algorithm were used to represent the fluorescence

689   intensities of various fluorophores (Meng et al., 2018). To evoke C1V1-mediated NE/DA

690   release, pulse trains (10-ms pulses at 20 Hz for 1 s) were delivered to the LC/SNc using a

691   561-nm laser with an output power of 9.9 mW measured at the end of the fiber.

Fiber photometry recording in mice during behavioral testing

693   For the experiments in Figure 7, a fiber photometry recording set-up was generated and

694   used as previously described (Falkner et al., 2016). GRAB$_{NE1m}$ was injected into the lateral

695   hypothalamus (Bregma AP: -1.7mm; ML: 0.90 mm   DV: -4.80 mm) of C57BL/6 mice in a

696   volume of 100 nl containing AAV9-hSyn-GRAB$_{NE1m}$ (Vigene, 1x10^{13} titer genomic copies

697   per ml) at 10 nl/min. A 400-μm optic fiber (Thorlabs, BFH48-400) housed in a ceramic

698   ferrule (Thorlabs, SFLC440-10) was implanted 0.2 mm above the injection site. The virus

699   was left to incubate for three weeks. Prior to fiber photometry recording, a ferrule sleeve

700   was used to connect a matching optic fiber to the implanted fiber. For recordings, a 400-

701   Hz sinusoidal blue LED light (30 μW; M470F1 driven by an LEDD1B driver; both from

702   Thorlabs) was bandpass-filtered (passing band: 472 ± 15 nm, Semrock, FF02-472/30-25)

703   and delivered to the brain in order to excite GRAB$_{NE1m}$. The emission light passed through

704   the same optic fiber, through a bandpass filter (passing band: 534 ± 25 nm, Semrock,

705   FF01-535/50), and into a Femtowatt Silicon Photoreceiver, which recorded the GRAB$_{NE1m}$

706   emission using an RZ5 real-time processor (Tucker-Davis Technologies). The 400-Hz

707   signals from the photoreceiver were extracted in real time using a custom program (Tucker-

708   Davis Technologies) and used to reflect the intensity of the GRAB$_{NE1m}$ fluorescence signal.

Behavioral assays

710   All behavioral tests were performed at least one hour after the onset of the dark cycle. For

711   the tail suspension test, each mouse was gripped by the tail and lifted off the bottom of its

712   cage six times for 60 s each, with at least one minute between each lift. For the forced

713   swim test, the mouse was gently placed in a 1000-ml conical flask containing lukewarm

714   water and removed after 4-6 minutes. After removal from the water, the mouse was gently

715   dried with paper towels and placed in the home cage on a heating pad. For conspecific
716   assays, an adult C57BL/6 group-housed mouse of either sex was placed inside the test
717   mouse's cage for 10 minutes. No sexual behavior or aggressive behavior was observed
718   during the interaction. For the food assay, ~4g of peanut butter was placed in the cap of a
719   15-ml plastic tube and placed inside of the test mouse's cage for 10 minutes. During that
720   period, the test mouse was free to explore, sniff, and eat the peanut butter. All videos were
721   acquired at 25 frames per second and manually annotated frame-by-frame using a custom
722   MATLAB program (Lin et al., 2011). "Contact" with the social stimulus refers to the period
723   in which the test mouse sniffed or was sniffed by the intruder. "Contact" with the peanut
724   butter refers to the period in which the test mouse sniffed or ate the peanut butter. "Lift"
725   refers to the period in which the experimenter gripped the mouse's tail and lifted the mouse
726   into the air.

727

728   **Quantification and statistical analysis**

729   For the imaging experiments using cultured HEK293T cells, primary neurons, and brain
730   slices, images were first imported to ImageJ software (National Institutes of Health) for
731   fluorescence intensity readouts, and then analyzed using MATLAB (MathWorks) with a
732   custom-written script or Origin Pro (OriginLab). The fluorescence response traces in the
733   brain slices shown in Figure 4 were processed with 3x binning and then plotted.

734   Time-lapse images of the zebrafish were analyzed using Fiji to acquire the
735   fluorescence intensity in the region of interest (ROI) in each frame. A custom-
736   written MATLAB program was then used to calculate the change in fluorescence
737   intensity ($\Delta F/F_0$) as follows: $\Delta F/F_0=(F_t-F_0)/F_0$, where F_t was the fluorescence intensity
738   at time t and F_0 was the average fluorescence intensity during the entire time window.
739   Statistical analyses were performed using GraphPad Prism 6 and Origin Pro (OriginLab).

740   For the fiber photometry data shown in Figure 7, the MATLAB function "msbackadj" with a
741   moving window of 25% of the total recording duration was first applied to obtain the
742   instantaneous baseline signal ($F_{baseline}$). The instantaneous $\Delta F/F$ was calculated as (F_{raw} −
743    $F_{baseline}$)/$F_{baseline}$, and a peri-stimulus histogram (PSTH) was calculated by aligning the $\Delta F/F$
744   signal of each trial to the onset of the behavior of interest. The response elicited during a
745   behavior was calculated as the average $\Delta F/F$ during all trials of a given behavior. The
746   response between behavioral periods was calculated as the average $\Delta F/F$ between two
747   behavioral episodes excluding 4 s immediately before the behavior's onset, as some
748   uncontrolled and/or unintended events (e.g., chasing the animal before the tail suspension
749   test) may have occurred during that period. The baseline signal was calculated as the
750   average $\Delta F/F$ 100 s prior to the start of the behavioral test. The peak response after each
751   drug injection was calculated as the average maximum $\Delta F/F$ during all tail suspension trials.
752   The decay time was calculated as the average time required to reach half of the peak
753   response.

22

754   Except where indicated otherwise, group differences were analyzed using the Student's *t*-

755   test, Wilcoxon matched-pairs signed rank test, Shapiro-Wilk normality test, one-way

756   ANOVA test, or Friedman's test. Except where indicated otherwise, all summary data are

757   presented as the mean ± SEM.

758

759   **Data and software availability**

760   The custom MATLAB programs using in this study will be provided upon request to the

761   corresponding author.

762

763

References

Akerboom, J., Chen, T.-W., Wardill, T.J., Tian, L., Marvin, J.S., Mutlu, S., Calderón, N.C., Esposti, F., Borghuis, B.G., Sun, X.R., *et al.* (2012). Optimization of a GCaMP Calcium Indicator for Neural Activity Imaging. The Journal of Neuroscience *32*, 13819.

Bast, N., Poustka, L., and Freitag, C.M. (2018). The locus coeruleus-norepinephrine system as pacemaker of attention - a developmental mechanism of derailed attentional function in autism spectrum disorder. Eur J Neurosci *47*, 115-125.

Berridge, C.W., Schmeichel, B.E., and Espana, R.A. (2012). Noradrenergic modulation of wakefulness/arousal. Sleep Med Rev *16*, 187-197.

Berridge, C.W., and Spencer, R.C. (2016). Differential cognitive actions of norepinephrine a2 and a1 receptor signaling in the prefrontal cortex. Brain Res *1641*, 189-196.

Berridge, C.W., and Waterhouse, B.D. (2003). The locus coeruleus–noradrenergic system: modulation of behavioral state and state-dependent cognitive processes. Brain Research Reviews *42*, 33-84.

Bito, L., Davson, H., Levin, E., Murray, M., and Snider, N. (1966). THE CONCENTRATIONS OF FREE AMINO ACIDS AND OTHER ELECTROLYTES IN CEREBROSPINAL FLUID, IN VIVO DIALYSATE OF BRAIN, AND BLOOD PLASMA OF THE DOG*. Journal of Neurochemistry *13*, 1057-1067.

Brodde, O.-E., Bruck, H., Leineweber, K., and Seyfarth, T. (2001). Presence, distribution and physiological function of adrenergic and muscarinic receptor subtypes in the human heart. Basic Research in Cardiology *96*, 528-538.

Bruns, D. (2004). Detection of transmitter release with carbon fiber electrodes. Methods *33*, 312-321.

Chefer, V.I., Thompson, A.C., Zapata, A., and Shippenberg, T.S. (2009). Overview of Brain Microdialysis. Current Protocols in Neuroscience *47*, 7.1.1-7.1.28.

Chrousos, G.P. (2009). Stress and disorders of the stress system. Nat Rev Endocrinol *5*, 374-381.

Chung, K.Y., Rasmussen, S.G., Liu, T., Li, S., DeVree, B.T., Chae, P.S., Calinski, D., Kobilka, B.K., Woods, V.L., Jr., and Sunahara, R.K. (2011). Conformational changes in the G protein Gs induced by the beta2 adrenergic receptor. Nature *477*, 611-615.

Espay, A.J., LeWitt, P.A., and Kaufmann, H. (2014). Norepinephrine deficiency in Parkinson's disease: the case for noradrenergic enhancement. Mov Disord *29*, 1710-1719.

Falkner, A.L., Grosenick, L., Davidson, T.J., Deisseroth, K., and Lin, D. (2016). Hypothalamic control of male aggression-seeking behavior. Nature Neuroscience *19*, 596.

Fenno, L., Yizhar, O., and Deisseroth, K. (2011). The development and application of optogenetics. Annu Rev Neurosci *34*, 389-412.

Goddard, A.W., Ball, S.G., Martinez, J., Robinson, M.J., Yang, C.R., Russell, J.M., and Shekhar, A. (2010). Current perspectives of the roles of the central norepinephrine system in anxiety and depression. Depress Anxiety *27*, 339-350.

Hashikawa, K., Hashikawa, Y., Falkner, A., and Lin, D. (2016). The neural circuits of mating and fighting in male mice. Current opinion in neurobiology *38*, 27-37.

Inoue, A., Ishiguro, J., Kitamura, H., Arima, N., Okutani, M., Shuto, A., Higashiyama, S., Ohwada, T., Arai, H., Makide, K., *et al.* (2012). TGFα shedding assay: an accurate and versatile method for detecting GPCR activation. Nature Methods *9*, 1021.

Jing, M., Zhang, P., Wang, G., Feng, J., Mesik, L., Zeng, J., Jiang, H., Wang, S., Looby, J.C., Guagliardo, N.A., *et al.* (2018). A genetically encoded fluorescent acetylcholine indicator for in vitro and in vivo

808   studies. Nature Biotechnology *36*, 726.

809   Justice, J.B. (1993). Quantitative microdialysis of neurotransmitters. Journal of Neuroscience
810   Methods *48*, 263-276.

811   Kroeze, W.K., Sassano, M.F., Huang, X.-P., Lansu, K., McCorvy, J.D., Giguère, P.M., Sciaky, N., and
812   Roth, B.L. (2015). PRESTO-Tango as an open-source resource for interrogation of the druggable
813   human GPCRome. Nature Structural &Amp; Molecular Biology *22*, 362.

814   Lee, G.J., Park, J.H., and Park, H.K. (2008). Microdialysis applications in neuroscience. Neurological
815   Research *30*, 661-668.

816   Leibowitz, S.F. (1970). Reciprocal Hunger-Regulating Circuits Involving Alpha-and Beta-
817   Adrenergic Receptors Located, Respectively, in the Ventromedial and Lateral Hypothalamus.
818   Proceedings of the National Academy of Sciences of the United States of America *67*, 1063-1070.

819   Leibowitz, S.F., Jhanwar-Uniyal, M., Dvorkin, B., and Makman, M.H. (1982). Distribution of α-
820   adrenergic, β-adrenergic and dopaminergic receptors in discrete hypothalamic areas of rat. Brain
821   Research *233*, 97-114.

822   Li, L., Feng, X., Zhou, Z., Zhang, H., Shi, Q., Lei, Z., Shen, P., Yang, Q., Zhao, B., Chen, S._, et al._ (2018).
823   Stress Accelerates Defensive Responses to Looming in Mice and Involves a Locus Coeruleus-
824   Superior Colliculus Projection. Curr Biol *28*, 859-871 e855.

825   Manglik, A., Kim, T.H., Masureel, M., Altenbach, C., Yang, Z., Hilger, D., Lerch, M.T., Kobilka, T.S.,
826   Thian, F.S., Hubbell, W.L._, et al._ (2015). Structural Insights into the Dynamic Process of beta2-
827   Adrenergic Receptor Signaling. Cell *161*, 1101-1111.

828   Marien, M.R., Colpaert, F.C., and Rosenquist, A.C. (2004). Noradrenergic mechanisms in
829   neurodegenerative diseases: a theory. Brain Research Reviews *45*, 38-78.

830   Marvin, J.S., Borghuis, B.G., Tian, L., Cichon, J., Harnett, M.T., Akerboom, J., Gordus, A., Renninger,
831   S.L., Chen, T.W., Bargmann, C.I._, et al._ (2013). An optimized fluorescent probe for visualizing
832   glutamate neurotransmission. Nat Methods *10*, 162-170.

833   McQuade, R., and Stanford, S.C. (2000). A microdialysis study of the noradrenergic response in rat
834   frontal cortex and hypothalamus to a conditioned cue for aversive, naturalistic environmental
835   stimuli. Psychopharmacology *148*, 201-208.

836   Meng, C., Zhou, J., Papaneri, A., Peddada, T., Xu, K., and Cui, G. (2018). Spectrally Resolved Fiber
837   Photometry for Multi-component Analysis of Brain Circuits. Neuron *98*, 707-717.e704.

838   Moore, R.Y., and Bloom, F.E. (1979). Central Catecholamine Neuron Systems: Anatomy and
839   Physiology of the Norepinephrine and Epinephrine Systems. Annual Review of Neuroscience *2*,
840   113-168.

841   Moret, C., and Briley, M. (2011). The importance of norepinephrine in depression. Neuropsychiatr
842   Dis Treat *7*, 9-13.

843   Muller, A., Joseph, V., Slesinger, P.A., and Kleinfeld, D. (2014). Cell-based reporters reveal in vivo
844   dynamics of dopamine and norepinephrine release in murine cortex. Nature Methods *11*, 1245.

845   Nakanishi, J., Takarada, T., Yunoki, S., Kikuchi, Y., and Maeda, M. (2006). FRET-based monitoring
846   of conformational change of the β2 adrenergic receptor in living cells. Biochemical and Biophysical
847   Research Communications *343*, 1191-1196.

848   Nygaard, R., Zou, Y., Dror, R.O., Mildorf, T.J., Arlow, D.H., Manglik, A., Pan, A.C., Liu, C.W., Fung, J.J.,
849   Bokoch, M.P._, et al._ (2013). The dynamic process of beta(2)-adrenergic receptor activation. Cell
850   *152*, 532-542.

851   Olive, M.F., Mehmert, K.K., and Hodge, C.W. (2000). Microdialysis in the mouse nucleus accumbens:

852 a method for detection of monoamine and amino acid neurotransmitters with simultaneous
853 assessment of locomotor activity. Brain Research Protocols *5*, 16-24.

854 Pacak, K., Palkovits, M., Kopin, I.J., and Goldstein, D.S. (1995). Stress-Induced Norepinephrine
855 Release in the Hypothalamic Paraventricular Nucleus and Pituitary-Adrenocortical and
856 Sympathoadrenal Activity: In Vivo Microdialysis Studies. Frontiers in Neuroendocrinology *16*, 89-
857 150.

858 Park, J., Kile, B.M., and Mark Wightman, R. (2009). In vivo voltammetric monitoring of
859 norepinephrine release in the rat ventral bed nucleus of the stria terminalis and anteroventral
860 thalamic nucleus. European Journal of Neuroscience *30*, 2121-2133.

861 Patriarchi, T., Cho, J.R., Merten, K., Howe, M.W., Marley, A., Xiong, W.-H., Folk, R.W., Broussard, G.J.,
862 Liang, R., Jang, M.J.*, et al.* (2018). Ultrafast neuronal imaging of dopamine dynamics with designed
863 genetically encoded sensors. Science *360*.

864 Rasmussen, S.G., Choi, H.J., Fung, J.J., Pardon, E., Casarosa, P., Chae, P.S., Devree, B.T., Rosenbaum,
865 D.M., Thian, F.S., Kobilka, T.S.*, et al.* (2011a). Structure of a nanobody-stabilized active state of the
866 beta(2) adrenoceptor. Nature *469*, 175-180.

867 Rasmussen, S.G., DeVree, B.T., Zou, Y., Kruse, A.C., Chung, K.Y., Kobilka, T.S., Thian, F.S., Chae, P.S.,
868 Pardon, E., Calinski, D.*, et al.* (2011b). Crystal structure of the beta2 adrenergic receptor-Gs protein
869 complex. Nature *477*, 549-555.

870 Ren, Q., Kurose, H., Lefkowitz, R.J., and Cotecchia, S. (1993). Constitutively active mutants of the
871 alpha 2-adrenergic receptor. Journal of Biological Chemistry *268*, 16483-16487.

872 Robinson, D.L., Hermans, A., Seipel, A.T., and Wightman, R.M. (2008). Monitoring Rapid Chemical
873 Communication in the Brain. Chemical Reviews *108*, 2554-2584.

874 Robinson, D.L., Venton, B.J., Heien, M.L.A.V., and Wightman, R.M. (2003). Detecting Subsecond
875 Dopamine Release with Fast-Scan Cyclic Voltammetry in Vivo. Clinical Chemistry *49*, 1763.

876 Schwarz, L.A., and Luo, L. (2015). Organization of the Locus Coeruleus-Norepinephrine System.
877 Current Biology *25*, R1051-R1056.

878 Schwarz, L.A., Miyamichi, K., Gao, X.J., Beier, K.T., Weissbourd, B., DeLoach, K.E., Ren, J., Ibanes, S.,
879 Malenka, R.C., Kremer, E.J.*, et al.* (2015). Viral-genetic tracing of the input–output organization of
880 a central noradrenaline circuit. Nature *524*, 88.

881 Shekhar, A., Katner, J.S., Sajdyk, T.J., and Kohl, R.R. (2002). Role of norepinephrine in the
882 dorsomedial hypothalamic panic response: An in vivo microdialysis study. Pharmacology
883 Biochemistry and Behavior *71*, 493-500.

884 Singleman, C., and Holtzman, N.G. (2014). Growth and Maturation in the Zebrafish, Danio Rerio: A
885 Staging Tool for Teaching and Research. Zebrafish *11*, 396-406.

886 Sokolowski, K., and Corbin, J.G. (2012). Wired for behaviors: from development to function of
887 innate limbic system circuitry. Frontiers in Molecular Neuroscience *5*, 55.

888 Sun, F., Zeng, J., Jing, M., Zhou, J., Feng, J., Owen, S.F., Luo, Y., Li, F., Wang, H., Yamaguchi, T.*, et al.*
889 (2018). A Genetically Encoded Fluorescent Sensor Enables Rapid and Specific Detection of
890 Dopamine in Flies, Fish, and Mice. Cell *174*, 481-496.e419.

891 Tanaka, M. (1999). Emotional Stress and Characteristics of Brain Noradrenaline Release in the Rat.
892 INDUSTRIAL HEALTH *37*, 143-156.

893 Urban, D.J., and Roth, B.L. (2015). DREADDs (designer receptors exclusively activated by designer
894 drugs): chemogenetic tools with therapeutic utility. Annu Rev Pharmacol Toxicol *55*, 399-417.

895 Vilardaga, J.-P., Bünemann, M., Krasel, C., Castro, M., and Lohse, M.J. (2003). Measurement of the

896 millisecond activation switch of G protein–coupled receptors in living cells. Nature Biotechnology
897 *21*, 807.

898 Wan, Q., Okashah, N., Inoue, A., Nehmé, R., Carpenter, B., Tate, C.G., and Lambert, N.A. (2018).
899 Mini G protein probes for active G protein-coupled receptors (GPCRs) in live cells. Journal of
900 Biological Chemistry.

901 Wang, A., Feng, J., Li, Y., and Zou, P. (2018a). Beyond Fluorescent Proteins: Hybrid and
902 Bioluminescent Indicators for Imaging Neural Activities. ACS Chemical Neuroscience *9*, 639-650.

903 Wang, H., Jing, M., and Li, Y. (2018b). Lighting up the brain: genetically encoded fluorescent
904 sensors for imaging neurotransmitters and neuromodulators. Curr Opin Neurobiol *50*, 171-178.

905 Watson, C.J., Venton, B.J., and Kennedy, R.T. (2006). In Vivo Measurements of Neurotransmitters
906 by Microdialysis Sampling. Analytical Chemistry *78*, 1391-1399.

907 Yang, T., and Shah, N.M. (2016). Molecular and neural control of sexually dimorphic social
908 behaviors. Current Opinion in Neurobiology *38*, 89-95.

909 Yao, Y., Li, X., Zhang, B., Yin, C., Liu, Y., Chen, W., Zeng, S., and Du, J. (2016). Visual Cue-
910 Discriminative Dopaminergic Control of Visuomotor Transformation and Behavior Selection.
911 Neuron *89*, 598-612.

912 Zhao, Y., Araki, S., Wu, J., Teramoto, T., Chang, Y.-F., Nakano, M., Abdelfattah, A.S., Fujiwara, M.,
913 Ishihara, T., Nagai, T.*, et al.* (2011). An Expanded Palette of Genetically Encoded Ca(2+) Indicators.
914 Science (New York, NY) *333*, 1888-1891.

915 Zhou, Z., and Misler, S. (1995). Amperometric detection of stimulus-induced quantal release of
916 catecholamines from cultured superior cervical ganglion neurons. Proceedings of the National
917 Academy of Sciences *92*, 6938.

918 Zimmerman, B.G. (1981). Adrenergic Facilitation by Angiotensin: Does it Serve a Physiological
919 Function? Clinical Science *60*, 343.

920 Zou, P., Zhao, Y., Douglass, A.D., Hochbaum, D.R., Brinks, D., Werley, C.A., Harrison, D.J., Campbell,
921 R.E., and Cohen, A.E. (2014). Bright and fast multicoloured voltage reporters via electrochromic
922 FRET. Nat Commun *5*, 4625.

923

924

925 **Figure 1. Design and optimization of genetically encoded NE sensors.**

926 (**A**) Selection of a candidate sensor scaffold by screening several NE-binding GPCRs.
927 Shown at the right are example images of the indicated chimeric GPCR-cpEGFP
928 candidates expressed in HEK293T cells. Yellow arrows indicate robust membrane
929 trafficking, and red arrows indicate impaired membrane trafficking. See also Figure S1.

930 (**B**) Identification of the most responsive NE sensor, NE0.5m (indicated by the black square)
931 by screening the cpEGFP insertion site in ICL3 of the α2AR. $\Delta F/F_0$ refers to the peak
932 change in fluorescence intensity in response to 100 μM NE.

933 (**C**) Optimizing the GRAB$_{NE}$ sensors by mutational screening of the insertion linker. NE0.5m
934 was used as a template, and the indicated amino acids on N-terminal and C-terminal sides
935 of the cpEGFP insert were mutated individually. Sensor NE1m (indicated by the pink
936 squares) was identified due to having the strongest response ($\Delta F/F_0$) and brightness
937 relative to the original NE0.5m sensor (indicated by the dashed line at 1.0).

938 (**D**) Tuning the sensor's affinity for NE by introducing mutations in the GPCR. Magnified
939 views of the ligand-binding pocket view from the cytosol are shown; key residues involved
940 in ligand binding and inducing a conformational change upon ligand binding are indicated.
941 The middle panel shows example images of HEK293T cells expressing the indicated
942 GRAB$_{NE}$ sensors; EGFP fluorescence is shown in the left column, and the fluorescence
943 response in the presence of 100 μM NE is shown in the right column. Shown at the right
944 are the normalized dose-response curves for the three GRAB$_{NE}$ sensors, with C$_{50}$ values
945 (top), and the average fluorescence change in response to 100 μM NE (bottom); n = 21-
946 67 cells from 3-5 cultures for each sensor.

947 The scale bars in (A) and (D) represent 10 μm.

948 ***$p < 0.001$ (Student's t-test).

949

Figure 2. Characterization of GRAB$_{NE}$ sensors in cultured cells.

(**A-C**) HEK293T cells were loaded with NPEC-NE, which was uncaged by photolysis with a pulse of 405-nm light. Uncaging caused a rapid increase in GRAB$_{NE1h}$ fluorescence, which was blocked in the presence of 10 µM yohimbine (YO). The data in A represent 3 trials each, and the data in C represent 7 cells from 3 cultures. The white dotted square indicates the image region and the purple square indicates the illumination region.

(**D-F**) NE was applied to HEK293T cells expressing GRAB$_{NE1m}$ or GRAB$_{NE1h}$ to measure τ_{on}. Yohimbine (YO) was then applied in order to measure τ_{off}; The white dotted line indicates the line-scanning region. n ≥ 6 cells from 6 cultures.

(**G**) The indicated compounds were applied to GRAB$_{NE1m}$ and GRAB$_{NE1h}$, and the change in fluorescence relative to NE is plotted.

(**H**) Dose-response curves for GRAB$_{NE1m}$, GRAB$_{NE1h}$, and wild-type α2AR for NE and DA, with EC$_{50}$ values shown; n ≥ 3 wells with 100-300 cells each.

(**I**) Fast-scan cyclic voltammetry measurements in response to increasing concentrations of NE and DA. The insets show exemplar cyclic voltammograms of NE and DA at 100 µM, with peak current occurring at ~0.6 V.

(**J**) Time course of ΔF/F$_0$ for GRAB$_{NE}$ sensors measured over a 2-h time frame; note that the fluorescent signal remained at the cell surface even after 180 min, indicating no measurable internalization or desensitization. n = 3 wells with 100-300 cells each.

(**K**) A TANGO assay was performed in order to measure β-arrestin–mediated signaling by GRAB$_{NE1m}$, GRAB$_{NE1h}$, and wild-type α2AR in the presence of increasing concentrations of NE; n = 4 wells with ≥10^5 cells each.

(**L,M**) GRAB$_{NE}$ sensors do not couple to downstream G protein signaling pathways. Wild-type α2AR, but not GRAB$_{NE1m}$ or GRAB$_{NE1h}$, drives Gαi signaling measured using a luciferase complementation assay (L). Disrupting of G protein activation with pertussis toxin does not affect the NE-induced fluorescence change in GRAB$_{NE1m}$ or GRAB$_{NE1h}$ (M). n = 3 wells with ≥10^5 cells each.

The scale bars in (A), (D), and (J) represent 10 µm.

*p < 0.05, **p < 0.01, and ***p < 0.001; n.s., not significant (Student's t-test).

29

Figure 3. Characterization of GRAB$_{NE}$ sensors in cultured neurons.

(**A-C**) GRAB$_{NE1m}$ is expressed in various plasma membrane compartment of cultured neurons. Cultured cortical neurons were co-transfected with GRAB$_{NE1m}$ and RFP-CAAX to label the plasma membrane, and the fluorescence response induced by bath application of NE was measured in the cell body, dendritic shaft and spine, and axon (**C**). n > 10 neurons from 4 cultures.

(**D,E**) Cultured cortical neurons expressing GRAB$_{NE1m}$ and GRAB$_{NE1h}$, but not GRAB$_{NEmut}$, respond to application of NE (10 μM). EGFP fluorescence and pseudocolor images depicting the response to NE are shown in (**D**), and the time course and summary of peak ΔF/F$_0$ are shown in (**E**). n > 15 neurons from 3 cultures.

(**F**) Dose-response curve for GRAB$_{NE}$ sensors expressed in cultured cortical neurons in response to NE and DA. n > 10 neurons from 3 cultures.

(**G**) Example trace (top) and summary (bottom) of cultured neurons transfected with GRAB$_{NE1m}$ and treated with the indicated compounds at 10 μM each. n = 9 neurons from 3 cultures.

(**H,I**) The fluorescence change in GRAB$_{NE1m}$ induced by 100 μM NE is stable for up to 1 h. Representative images taken at the indicated times are shown in (**H**). An example trace and summary data are shown in (**I**). Where indicated, 10 μM yohimbine (YO) was added. n = 11 neurons from 3 cultures.

The scale bars in (**A**) and (**B**) represent 10 μm; the scale bars in (**D**) and (**H**) represent 25 μm.

***$p < 0.001$; n.s., not significant (Student's t-test).

Figure 4. Release of endogenous NE measured in mouse brain slices.

(**A**) **Left**, schematic illustration of the slice experiments. An AAV expressing hSyn-NE1m was injected into the LC; two weeks later, acute brain slices were prepared and used for electric stimulation experiments. **Right**, exemplar 2-photon microscopy images showing the distribution of $GRAB_{NE1m}$ in the plasma membrane of LC neurons.

(**B**) **Left and middle**, representative pseudocolor images and corresponding fluorescence changes in $GRAB_{NE1m}$-expressing neurons in response to 2, 20, and 100 pulses delivered at 20 Hz. The ROI (50-µm diameter) for data analysis is indicated in the images. **Right**, summary of the peak fluorescence change in slices stimulated as indicated; n = 5 slices from 5 mice.

(**C**) Exemplar traces and summary data of $GRAB_{NE1m}$-expressing neurons in response to 20 electrical stimuli delivered at 20 Hz in ACSF, 4-AP (100 µM), or 4-AP with Cd^{2+} (100µM); n = 4 slices from 4 mice.

(**D**) Kinetic properties of the electrically evoked fluorescence responses in $GRAB_{NE1m}$-expressing LC neurons. **Left**, image showing a $GRAB_{NE1m}$-expressing LC neuron for line scan analysis (red dashed line). **Middle and right**, example trace and summary of the responses elicited in $GRAB_{NE1m}$-expressing neurons before, and after 10 pulses delivered at 100Hz; n = 4 slices from 4 mice.

(**E**) The norepinephrine transporter blocker desipramine (Desi, 10 µM; red) increases the effect of electrical stimuli (20 pulses at 20 Hz) or two trains of stimuli with a 1-s interval compared to ACSF (black traces). n = 5 slices from 5 mice.

(**F**) The fluorescence response in $GRAB_{NE1m}$-expressing neurons is stable. Eight stimuli (20 pulses at 20 Hz) were applied at 5-min intervals, and the response (normalized to the first train) is plotted against time. n = 5 slices from 5 mice.

(**G**) Traces and summary data of the fluorescence response measured in neurons expressing $GRAB_{NE1m}$, $GRAB_{NEmut}$, or $GRAB_{DA1m}$ in response to 20 pulses delivered at 20 Hz in the presence of ACSF or 20 µM YO; n = 3-7 slices from 3-7 mice.

(**H**) Traces and summary data of the fluorescence response measured in neurons expressing $GRAB_{NE1m}$ or $GRAB_{DA1m}$. Where indicated, 50 µM NE, 50 µM DA, 20 µM yohimbine (YO), and/or 20 µM haloperidol (Halo) was applied to the cells. n = 3-5 slices from 3-5 mice.

The scale bars represent 10 µm.

*$p < 0.05$, **$p < 0.01$, and ***$p < 0.001$; n.s., not significant (Student's *t*-test).

1036 **Figure 5. GRAB$_{NE1m}$ can be used to measure noradrenergic activity *in vivo* in**
1037 **transgenic zebrafish.**

1038 (**A**) *In vivo* confocal image of a Tg(HuC:GRAB$_{NE1m}$) zebrafish expressing GRAB$_{NE1m}$ in
1039 neurons driven by the HuC promoter. Larvae at 6 days post-fertilization were used.

1040 (**B-D**) Bath application of NE (50 µM) but not DA (50 µM) elicits a significant increase in
1041 fluorescence in the tectal neuropil of Tg(HuC:GRAB$_{NE1m}$) zebrafish, but not in GRAB$_{NEmut}$
1042 zebrafish, and this increase is blocked by YO (50 µM), but not ICI 118,551 (50 µM). n = 7.

1043 (**E-H**) Visual looming stimuli evoke the release of endogenous NE in the midbrain of
1044 GRAB$_{NE1m}$ zebrafish, but not in GRAB$_{NEmut}$ zebrafish. The looming stimuli paradigm is
1045 shown in the left of (**E**). Where indicated, YO (50 µM) or ICI 118,551 (50 µM) was
1046 applied. Desipramine (Desi, 50 µM) application slowed the decay of looming-induced NE
1047 release (**H**). n = 6 for GRAB$_{NEmut}$ and n = 9 for the others.

1048 (**I-K**) Single-cell labeling of GRAB$_{NE1m}$ in the midbrain of zebrafish larva (**I**), with looming-
1049 evoked responses shown in (**I** and **J**). The summary data for 6 labeled cells are shown in
1050 (**K**).

1051 The scale bar shown in (**A, left**) represents 10 µm; the scale bars shown in (**A, right**), (**B**)
1052 and (**E**) represent 50 µm. The scale bar shown in (**I**) represents 5 µm.

1053 *$p < 0.05$, **$p < 0.01$, ***$p < 0.001$, and ****$p < 0.0001$; n.s., not significant (Wilcoxon
1054 matched-pairs signed rank test in panel **H**, all others were analyzed using the paired or
1055 unpaired Student's *t*-test).
1056

1057 **Figure 6. GRAB$_{NE1m}$ can be used to measure optogenetically stimulated**
1058 **noradrenergic activity *in vivo* in freely moving mice.**

1059 (**A**) Schematic illustration depicting the experimental design for recording GRAB$_{NE1m}$ and
1060 GRAB$_{NEmut}$ fluorescence in response to optical stimulation of C1V1 in the locus coeruleus
1061 (LC).

1062 (**B**) Representative traces of optogenetically stimulated GRAB$_{NE1m}$ (top) and GRAB$_{NEmut}$
1063 (bottom) activity in the LC before (baseline, left), 15 min after an i.p. injection of the NET
1064 blocker desipramine (10 mg/kg, middle), and 15 min after an i.p. injection of the α2AR
1065 antagonist yohimbine (2 mg/kg, right). The vertical tick marks indicate the optogenetic
1066 stimuli. Black arrows represent the timing for grabbing and i.p. injection.

1067 (**C-D**) Average traces of GRAB$_{NE1m}$ fluorescence (**C**), summary data (**D**), and the decay
1068 time constant (**E**) in response to optical stimulation in the LC following treatment with the
1069 indicated compounds. n = 15 trials from 3 mice for each condition.

1070 (**F,G**) Schematic illustration (**F, left**), representative traces (**F, right**), average
1071 fluorescence change (**G, left**), and summary data (**G, right**) for GRAB$_{NE1m}$ in response to
1072 optical stimulation of noradrenergic neurons in the LC and dopaminergic neurons in the
1073 SNc.

1074 ***$p < 0.001$ (for D and E, One-Way ANOVA, for G, Student's *t*-test).
1075
1076

Figure 7. GRAB$_{NE1m}$ can be used to measure noradrenergic activity in the hypothalamus during stress, food-related behavior, and social interaction.

(**A**) Schematic diagrams depicting the fiber photometry recording, virus injection, and recording sites.

(**B**) Histology showing the expression of GRAB$_{NE1m}$ (green) and placement of the recording; the nuclei were counterstained with DAPI (blue). Scale bar: 500µm.

(**C1-E6**) Representative traces (**C1-C6**), average per-stimulus histograms (**D1-D6**), and summary data (**E1-E6**) showing normalized GRAB$_{NE1m}$ fluorescence (ΔF/F) before and during the forced swim test (**1**), the tail suspension test (**2**), the hand presentation test (**3**), social interaction with an intruder of the opposite sex (**4**) and the same sex (**5**), and presentation of peanut butter (**6**). n = 3 animals each.

(**F**) Representative traces of GRAB$_{NE1m}$ fluorescence during the tail suspension test 10 minutes after saline injection, 25 minutes after atomoxetine (ATX) or yohimbine (YO) injection, and 15 minutes after GBR 12909 or sulpiride (Sul) injection.

(**G-I**) Average peri-stimulus histograms (**H**), peak change in GRAB$_{NE1m}$ fluorescence, and post-test decay time measured during the tail suspension test after injection of the indicated compounds. n = 3 each.

The Shapiro-Wilk normality test was performed; if the test revealed that the followed a normal distribution, a paired Student's *t*-test or one-way repeated measures ANOVA followed by Tukey's multiple comparisons was performed. If the values did not follow a normal distribution, a non-parametric ANOVA (Friedman's test) was performed followed by Dunn's multiple comparisons test. In (**C**) and (**D**), the blue dotted lines represent the start of the stimulus, and the red dotted lines represent the end of the trial.

*$p < 0.05$ and **$p < 0.01$.

Figure S1. Characterization of the membrane trafficking of a panel of screening candidates (related to Fig. 1).

Representative images (**A**) of HEK293T cells co-transfected with the indicated screening candidates (green) together with RFP-CAAX (red) to label the plasma membrane. KDELR-EGFP was used as an ER marker. The dashed white lines indicate the line used for the line-scanning data shown in (**B**) and summarized in

(**C**) n = 30 cells from 4-5 cultures.

The scale bars in (**A**) represent 10 μm.

*$p < 0.05$ and ***$p < 0.001$; n.s., not significant (Student's *t*-test).

1112 **Figure S2. Further characterization of GRAB$_{NE}$ sensors (related to Fig. 2).**

1113 (**A**) Fluorescence intensity of GRAB$_{NE1m}$ and GRAB$_{NE1h}$ expressed relative to EGFP-α2AR.
1114 n ≥ 2 wells with 300-500 cells per well.

1115 (**B**) G protein activation mediated by GRAB$_{NE1m}$ and wild-type α2AR was measured using
1116 the TGFα shedding assay and is expressed relative to α2AR. n = 4 wells with ≥10^5 cells
1117 per well.

1118 (**C**) Exemplar (**left**) and summary data (**right**) showing the photostability of GRAB$_{NE}$
1119 sensors and EGFP-CAAX using confocal (**top**) and 2-photon (**bottom**) microscopy. n > 10
1120 cells from at least 3 cultures.

1121 (**D**) Exemplar cyclic voltammograms for 10 µM NE (**top**), 10 µM DA (**middle**), and 10 µM
1122 Glu (**bottom**) measured using FSCV are shown. The traces were averaged from separate
1123 200 trials.

1124 ***$p < 0.001$ (Student's *t*-test).

1125

Figure S3. GRAB$_{NE}$ sensors respond selectively to noradrenergic agonists in brain slices (related to Fig. 4).

(**A**) Schematic drawing showing the experimental design for measuring CA1 pyramidal neurons in cultured rat hippocampal slices.

(**B**) Heat-map images of the change in fluorescence in GRAB$_{NE1m}$-expressing CA1 neurons in response to a 10-ms local application of NE (20 µM). The red and orange traces show the fluorescence responses of two neurons, and the green trace shows the average response of all neurons in the field. The scale represents 20 µm.

(**C**) Fluorescence responses measured in GRAB$_{NE1m}$-, GRAB$_{NE1h}$-, and GRAB$_{NEmut}$-expressing CA1 neurons following a 10-ms puff (arrow) of ACSF, NE (20 µM), Epi (100 µM), or brimonidine (UK, 20 µM).

(**D**) Maximum $\Delta F/F_0$ response measured in GRAB$_{NE1m}$-, GRAB$_{NE1h}$-, and GRAB$_{NEmut}$-expressing CA1 neurons following a 10-ms puff of ACSF or NE. n = 20-21 cells from 8 animals per group.

(**E**) Rise times and decay time constants were measured in CA1 neurons expressing GRAB$_{NE1m}$- and GRAB$_{NE1h}$- expressing CA1 neurons in response to a puff of NE. n = 21 cells from 8 animals.

(**F**) Maximum $\Delta F/F_0$ response measured in GRAB$_{NE1m}$-expressing CA1 neurons following a puff of NE, Epi, or brimonidine (UK). n = 20-21 cells from 8 animals per group.

(**G**) Rise times and decay time constants were measured in GRAB$_{NE1m}$-expressing CA1 neurons following a puffs of Epi or brimonidine (UK).

(**H**) Schematic illustration depicting AAV-mediated delivery of GRAB$_{NE1h}$ in the mouse hippocampus and bath application of various agonists in the dentate gyrus.

(**I**) Example images showing GRAB$_{NE1h}$ (green) expression and dopamine beta hydroxylase (DBH) immunostaining (red) in the dentate gyrus of AAV-GRAB$_{NE1h}$- and control-injected hippocampi. The nuclei were counterstained with DAPI. The scale bar represents 100 µm.

(**J**) Electrical stimulation evokes NE release in the hippocampus measured as a change in GRAB$_{NE1h}$ fluorescence. The response was blocked by batch application of yohimbine (YO). Exemplar images (**left**), representative traces (**middle**), and the summary data (**right**) are shown.

(**K**) Normalized change in GRAB$_{NE1h}$ fluorescence in response to bath application of the indicated noradrenergic agonists in the presence or absence of ICI 118,551 or yohimbine.

The scale bar shown in (**B**) represents 20 µm; the scale bar shown in (**I**) represents 100 µm. The scale bar shown in (**J**) represents 10 µm.
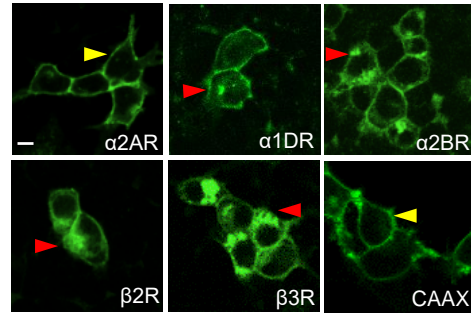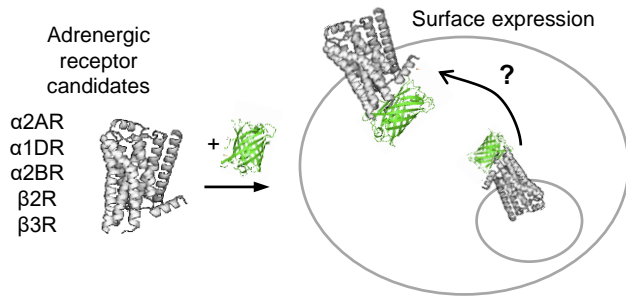
1161   *$p < 0.05$ and ***$p < 0.001$; n.s., not significant (Student's *t*-test, Wilcoxon test, or Mann-
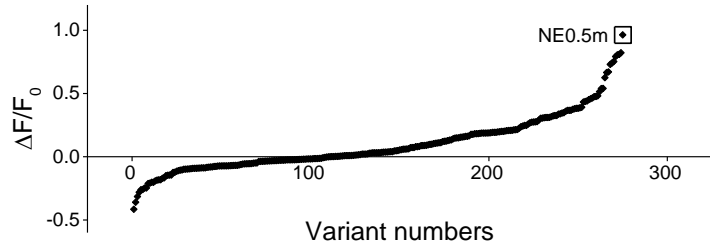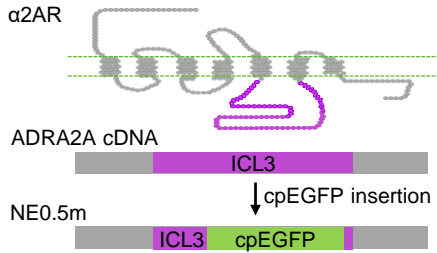
1162   Whitney rank sum test).

1163

1164

Fig 1
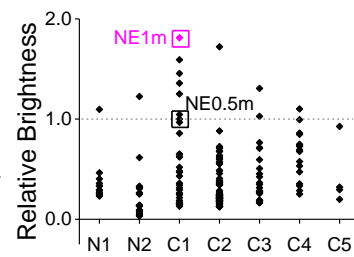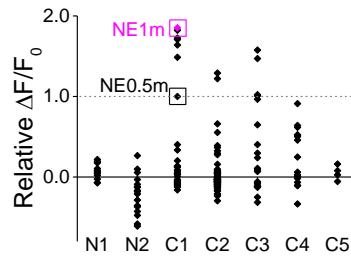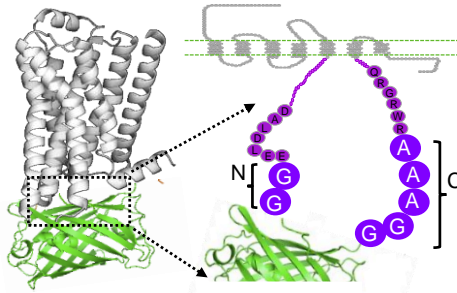
A. Selection of NE sensitive GPCR

B. Insertion sites screening

C. Optimization of coupling linkers

D. Affinity tuning of NE sensors
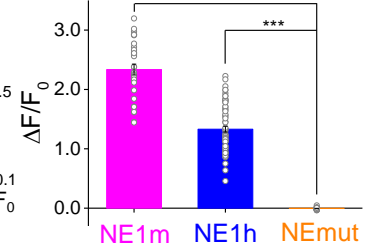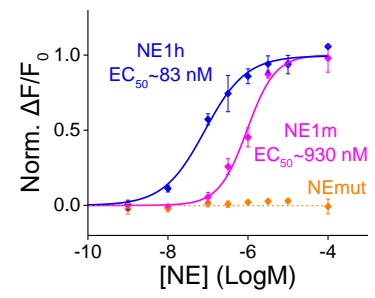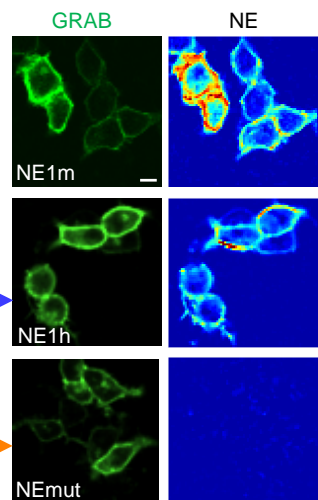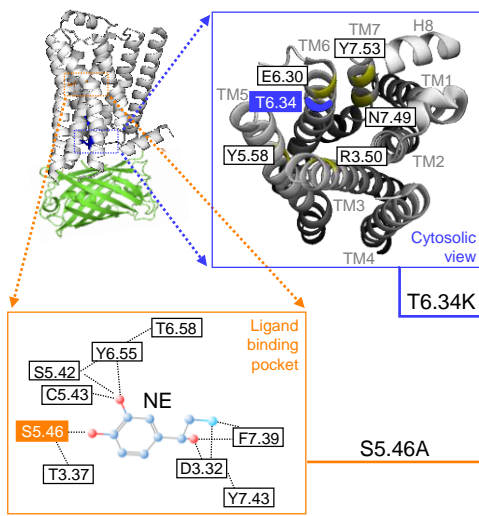
Fig 2

A Photolysis

NE1h

caged-NE

hv ↓ uncage

NE + NPEC

B On kinetics

NE1h τ_{on} ~ 130 ms

caged-NE

caged-NE + YO

C

| uncage | + | + |
| YO | - | + |

137 ms

τ_{on}

D Rapid perfusion

GRAB$_{NE}$

E On kinetics

NE1m

NE1m τ_{on} ~ 69 ms

NE1h

NE1h τ_{on} ~ 29 ms

Off kinetics

NE1m τ_{off} ~ 750 ms

NE1h τ_{off} ~ 2.0 s

F

34 ms   72 ms   36 ms   680 ms   1890 ms

Ctrl dye   NE1m   NE1h   NE1m   NE1h

τ_{on} τ_{off}

G All at 10 μM, except ICI 5 μM, YO 2 μM

NE1m

NE1h

NE Epi UK ISO NE+YO NE+ICI 5-HT ACh Glu GABA ADO His Gly TA

H

NE1m

NE EC$_{50}$~1 μM

DA EC$_{50}$~350 μM

>350-fold

NE1h

NE EC$_{50}$~0.1 μM

DA EC$_{50}$~3.7 μM

37-fold

WT-α2AR

NE EC$_{50}$~0.02 μM

DA EC$_{50}$~1.7 μM

85-fold

I FSCV

DA

NE

J

With NE 0min   With NE 120min

n.s.

Time (min)

K Tango Assay

WT-α2AR EC$_{50}$~11 nM

NE1m

NE1h

L Luciferase Complement. Assay

WT-α2AR EC$_{50}$ ~ 4 μM

NE1m EC$_{50}$ ~ 1 mM

NE1h

M PTX treatment

NE1h EC$_{50}$ w/o PTX~38 nM

w/ PTX~41 nM

NE1m EC50 w/o PTX~650 nM

w/ PTX~660 nM

Fig 3

A

NE1m

B

NE1m+RFP-CAAX | Overlay | NE1m | CAAX

NEmut+RFP-CAAX | Overlay | NEmut | CAAX

C

D

GRAB | NE

NE1m

NE1h

NEmut

$\Delta F/F_0$

E

10 μM NE

NE1m
NE1h
NEmut

F

NE1m

NE
$EC_{50}\sim1.9$ μM

DA
$EC_{50}\sim1.4$ mM

NE1h

NE
$EC_{50}\sim93$ nM

DA
$EC_{50}\sim600$ nM

NEmut
NE

G

NE Epi   All at 10 μM   NE
                                    YO

ISO 5HT DA His

n.s.

***   ***

NE(1st) Epi ISO 5HT DA His NE(2nd) NE+YO

H

0 min | NE 2min

NE 50min | YO 60min

I

100 μM NE

YO

n.s.   ***

0 min 2 min 50 min 60 min YO

Fig 4

Fig 5

A Zoom in — Tg(HuC:NE1m), 6 dpf

Forebrain 1

4 Midbrain 2

Hindbrain 3

Spinal cord

B Midbrain

Before 4

NE

NE+YO

C Tectal Neuropil

50 µM NE

50 µM YO

NE1m — 0.25 ΔF/F₀ / 100 s

50 µM DA — NE1m

50 µM NE — NEmut / 100 s

D ΔF/F₀ — NE, NE+YO, DA (NE1m), NE (NEmut) — ** ** ***

E Looming — Control

Before

Looming

After

F 0.1 ΔF/F₀ / 50 s

Control

ICI(βAR antagonist)

YO(αAR antagonist)

NEmut

Looming stimuli — 90 s — 5 s

G ΔF/F₀ — Control, ICI (NE1m), YO, Control (NEmut) — n.s. ** *** **

H Desi / Control — 0.04 ΔF/F0 / 20 s — Looming

Decay τ_off (s) — Ctrl, Desi — *

I NE1m — Before — Looming — After

J 0.1 ΔF/F₀ / 50 s

Looming stimuli — 90 s — 5 s

K ΔF/F₀ — looming − + — Cell # 1 2 3 4 5 6 — **** *** *** **** **** ***

Fig 6

A

473nm laser for Recording
561nm laser for Stimulation

C1V1 **LC**
NE1m/NEmut

B

| Baseline | 10 mg/kg Desi | 2 mg/kg YO |

20 pulses, 1 s   1min

10% ΔF/F$_0$ 5 min

NE1m

NEmut

Grabbing & i.p. injection

C

Baseline   Desi (NET blocker)   YO (α2AR antagonist)   GBR (DAT blocker)   Etic (D2R antagonist)

ΔF/F$_0$ (%)   Time (s)

D

NE1m   NEmut

ΔF/F$_0$ (%)

***

Baseline   Desi   YO   GBR   Etic   Baseline   Desi   YO

E

NE1m

Decay time constant (s)

***

Baseline   Desi   GBR   Etic

F

473nm laser for Recording
561nm laser for Stimulation

SNc   LC
NE1m C1V1

5% ΔF/F$_0$ 30 s

Stimulating NE neurons and record in LC

Stimulating DA neurons and record in SNc

G

20 pulses, 1 s

ΔF/F$_0$ (%)   LC

SNc   Time (s)

ΔF/F$_0$ (%)   ***

LC   SNc

Fig 7

A Photoreceiver · 535 nm · Dichroic · 470 nm LED · Optic fiber · Hypothalamus · WT · hSyn · NE1m · pA

B DAPI · NE1m · Hypothalamus · Fiber

C1 Actively move — Forced Swim test (s)
C2 Lift — Tail suspension test (s)
C3 Hand in cage — Hand presentation test (s)
C4 Opposite sex — Interact with intruder — Introduce opposite sex intruder (s)
C5 Same sex — Interact with intruder — Introduce same sex intruder (s)
C6 Contact peanut butter — Introduce peanut butter (s)

D1 n = 3 — Time in water(s)
D2 Lift onset (s)
D3 Hand in cage (s)
D4 Interact onset (s)
D5 Interact onset (s)
D6 Contact peanut butter (s)

E1 n = 3 — ** — Basel / FST
E2 * — Base / Between / Lift
E3 * — Base / Between / Hand
E4 Base / Between / Interact
E5 Base / Between / Interact
E6 Base / Between / Contact

F1 Tail suspension test — Saline — 3 mg/kg ATX (NET inhibitor) — 2 mg/kg YO (α2 antagonist)
F2 Saline — 10 mg/kg GBR (DAT inhibitor) — 50 mg/kg Sul (D2R inhibitor)

G1 n = 3 — Lift onset (s)
G2 Lift onset (s)

H1 n = 3 — * — Saline / ATX / YO
H2 n = 3 — Saline / GBR / Sul

I1 n = 3 — ** — Decay time (s) — Saline / ATX / YO
I2 n = 3 — Decay time (s) — Saline / GBR / Sul

Fig S1

A

EGFP | RFP-CAAX | Overlay

α1DR-cpEGFP

α2AR-cpEGFP

α2BR-cpEGFP

β2R-cpEGFP

β3R-cpEGFP

KDELR-EGFP

EGFP-CAAX

NE1m

NE1h

NEmut

B

Norm. Intensity
5 μm

C Norm. Pearson R

0.0   0.5   1.0

***

n.s.

***

*

n.s.

*

n.s.

n.s.

Fig S2

A

B

TGFα shedding Assay

WT-α2AR
EC_{50}~23 nM

NE1m
EC_{50}~1.9 μM

[NE] (LogM)

C

1-Photon (Confocal)

EGFP-CAAX
NE1m
NE1h

*** ***

2-Photon

*** ***

EGFP-CAAX   NE1m   NE1h

D

NE

DA

Glu

Fig S3

A — NE1m, NE1h or NEmut (by Sindbis virus) — Cultured slice preparation — 18 hrs *in vitro* — Imaging — Camera, Puff pipette

B — Relative ΔF (%) 0–100, Cell 1, Cell 2, Average, 20% ΔF/F$_0$, 10 sec

C — NE, ACSF | NE, Epi, UK — NE1m, NE1h, NEmut, NE1m, NE1m — 5% ΔF/F$_0$, 20 sec

D — ACSF, NE — ΔF/F$_0$ (%), NE1m, NE1h, NEmut — *, *, n.s.

E — NE1m, NE1h — Rise Time (s), τ_{Decay} (s) — n.s., *

F — NE, Epi, UK — ΔF/F$_0$ (%) — n.s., n.s.

G — Epi, UK — Rise Time (s), τ_{Decay} (s) — *, *

H — ITR hSyn tTA WPRE pA ITR / TRE GRAB$_{NE}$ WPRE pA — AAV9-hSyn-tTA, AAV9-TRE-GRAB$_{NE}$ — Hippocampus, LC — Electrical stimulation, stimulation electrode, Hippocampus, Bregma:-1.8mm

I — GRAB (GFP), DBH, DAPI, Merge — NE1h, Non-injection control

J — NE1h, ACSF, YO, -0.1 ΔF/F$_0$ 1 — 20 Hz, 1 s, 5% ΔF/F$_0$ 10 s — ΔF/F$_0$, ACSF, YO, NE1h, ***

K — Normalized ΔF/F$_0$ — NE, UK, Epi, ISO, NE, UK, Epi, ISO, NE, UK, Epi, ISO — ICI, YO